UNIVERSITÀ POLITECNICA DELLE MARCHE

FACOLTÀ DI INGEGNERIA

Master's Degree in BIOMEDICAL ENGINEERING

Curriculum: Engineering of Medical Devices

ELECTROENCEPHALOGRAPHIC ANALYSIS FOR CLASSIFICATION OF MOTOR EXECUTION AND MOTOR IMAGERY IN A HEALTHY POPULATION

Supervisor:

Dott. **Ilaria Marcantoni**

Candidate:

Johana Gogo

Co-supervisor:

Prof. **Laura Burattini**

Dott. **Erica Iammarino**

Academic Year: 2025-2026

ABSTRACT

The brain regulates bodily functions, including movement, cognition, and sensory processing, through neurons and glial cells. Motor execution and motor imagery represent two complementary conditions that share overlapping neural substrates, yet differ in the presence or absence of overt motor output. Beyond this fundamental distinction, they are known to exhibit a range of electrophysiological differences which we aim to capture and exploit through a comprehensive set of EEG-derived features. Understanding the electrophysiological differences between these conditions is essential for the development of reliable brain–computer interfaces (BCIs) for motor rehabilitation and assistive technologies. Electroencephalography (EEG) is a key tool for studying brain activity, offering insights into motor-related cortical dynamics and mental states. The aim of this study is to investigate EEG-derived features that can be used to discriminate between motor execution and motor imagery, exploiting machine learning techniques. To do so we have analyzed the EEG data of a healthy population during motor execution and motor imagery tasks coming from 109 subjects, part of a freely available database on PhysioNet, specifically designed to support research investigating motor-related cortical activity. The tasks performed include execution and imagery of right hand, left hand, both fists, and both feet movements. EEG recordings were preprocessed using EEGLAB software and to ensure that the data were clean, sliding windows were extracted and the noisy ones were removed. The preprocessing involved 0.5–70 Hz band-pass filtering, average-based re-referencing, and artifact removal after independent component analysis using the ICLabel plug-in. Then, EEG rhythms were extracted and their powers computed, and 22 engagement indexes were computed according to the review of Marcantoni et al. In addition, event-related desynchronization (ERD) in the alpha and beta bands, frontal alpha asymmetry, and connectivity measures like coherence and phase-locking value, were extracted. Then, for each of the four movement types considered, we were able to develop classification models using four different classifiers: Linear Discriminant Analysis, Support Vector Machine with linear and radial basis function kernels, and Random Forest. Model performance was evaluated using both 10-fold cross-validation and leave-one-subject-out cross-validation. The Random Forest classifier consistently outperformed the other models, achieving 10-fold cross-validation accuracies ranging from 62.53% to 67.13% using region-aggregated features. The feet movement yielded the highest performance, with an accuracy of 67.13% and an F1-score of 61.68%. However, performance was considerably lower under leave-one-subject-out cross-validation (52.14–53.62% accuracy), highlighting the critical challenge of cross-subject generalization. It should be noted that even the 10-fold cross-validation accuracies,

although above chance, remained moderate, indicating that the classification task is inherently complex. This finding underscores the importance of considering subject-specific variability and the need to incorporate robust feature extraction and domain adaptation strategies in motor imagery classification tasks. This study also highlighted the complexity of using EEG for motor decoding, showing that an approach that accounts for a wide array of features is crucial to develop accurate and generalizable models. The significant role of machine learning techniques like Random Forest further emphasizes their potential in handling high-dimensional data and selecting the most informative features, while also stressing the need for advanced domain generalization methods to overcome inter-subject variability and improve the reliability of BCI systems.

CONTENTS

1. INTRODUCTION

1.1 FUNDAMENTALS OF THE HUMAN NERVOUS SYSTEM

The nervous system is essential for regulating and coordinating bodily functions. At the core of its operation are neurons, specialized cells that transmit electrical impulses, and glial cells, which support and maintain the neuron function. The brain, as the primary control center, is crucial in processing sensory information and generating responses. The human nervous system serves a dual purpose: it enables interaction with the external environment while simultaneously regulating a vast array of internal physiological processes, including metabolic functions. To accomplish these tasks, the nervous system acquires information via sensory pathways, integrates and elaborates this input, and subsequently generates appropriate responses, such as muscle contraction or the perception of pain. From an anatomical perspective, the nervous system is partitioned into two main components: the central nervous system (CNS) and the peripheral nervous system (PNS). The CNS includes all the nervous tissue contained in the brain and spinal cord, on the other hand, the PNS consists of all nerves that enter or exit from the brain and spinal cord. The PNS is further subdivided based on the direction of signal propagation: afferent neurons convey information from the periphery toward the CNS, so they transduce specific physical or chemical stimuli into graded or action potentials; efferent neurons carry commands from the CNS to effector organs [1].

1.1.1 Anatomy of the Human Brain

The brain is the central controlling organ of the human being, it is composed of several different regions, each with specialized functions. The adult human brain weights about 1.3-1.4 kg [1]. Array tomography showed that the number of neurons in the adult human brain is about 86 billion. Of these, 19% are in the cerebral cortex and subcortical white matter, 80% are in the cerebellum, and 1% in the rest of the brain [2]. The brain, illustrated in Figure 1, can be divided into three main regions: the hindbrain, the midbrain and the forebrain. The hindbrain and the midbrain together form the brainstem. The hindbrain, besides the lower part of the brainstem, includes also the upper part of the spinal cord and the cerebellum. The midbrain controls some reflex actions and is part of the circuit involved in the control of eye movements and other voluntary movements. Specifically, the midbrain is composed by the superior and inferior colliculi. The superior colliculi play an important role in the visual pathway, while the inferior colliculi are important in the auditory pathway. In general, the midbrain integrates sensory information from the eyes and the ears with the muscle movements: the information from eyes and ears are used to refine movements. The hindbrain controls the body's vital

functions such as respiration and heart rate. The forebrain is the source of intellectual activities, and it includes the thalamus, the hypothalamus and the cerebrum. The thalamus, through connections with different areas of the cerebral cortex, is involved in the functioning of all sensory systems: every sensory system, but the olfactory system, has a thalamic nucleus that receives sensory signals and forwards them to the related primary cortical area. It also plays a fundamental role in voluntary movements, in the regulation of the sleep-wake cycle, in the state of consciousness, in emotions and in some aspects of memory capacity. The hypothalamus is the anatomical element of connection between the nervous system and the endocrine system. Connected to the reticular formation of the brainstem and to the amygdala, the hypothalamus takes part in the regulation of body temperature or the sense of satiety, and in the release of hormones. The amygdala is a paired nuclear complex, located medially within the temporal lobes. It has a fundamental role in decision-making, processing of memory and emotional responses, in particular fear, anxiety and aggression. The cerebrum is the largest and most specialized part of the forebrain. It controls skeletal muscles, thinking, intelligence, language and emotion. The cerebrum has a more superficial layer, called the cerebral cortex, and a deeper component, called the subcortical component. The cerebral cortex is pure grey matter, while the subcortical component includes both grey matter structures and white matter structures [1]. The cerebral cortex has a large surface and is convoluted resulting in gyri and sulci, to enable more cerebral cortex matter to fit inside the skull.

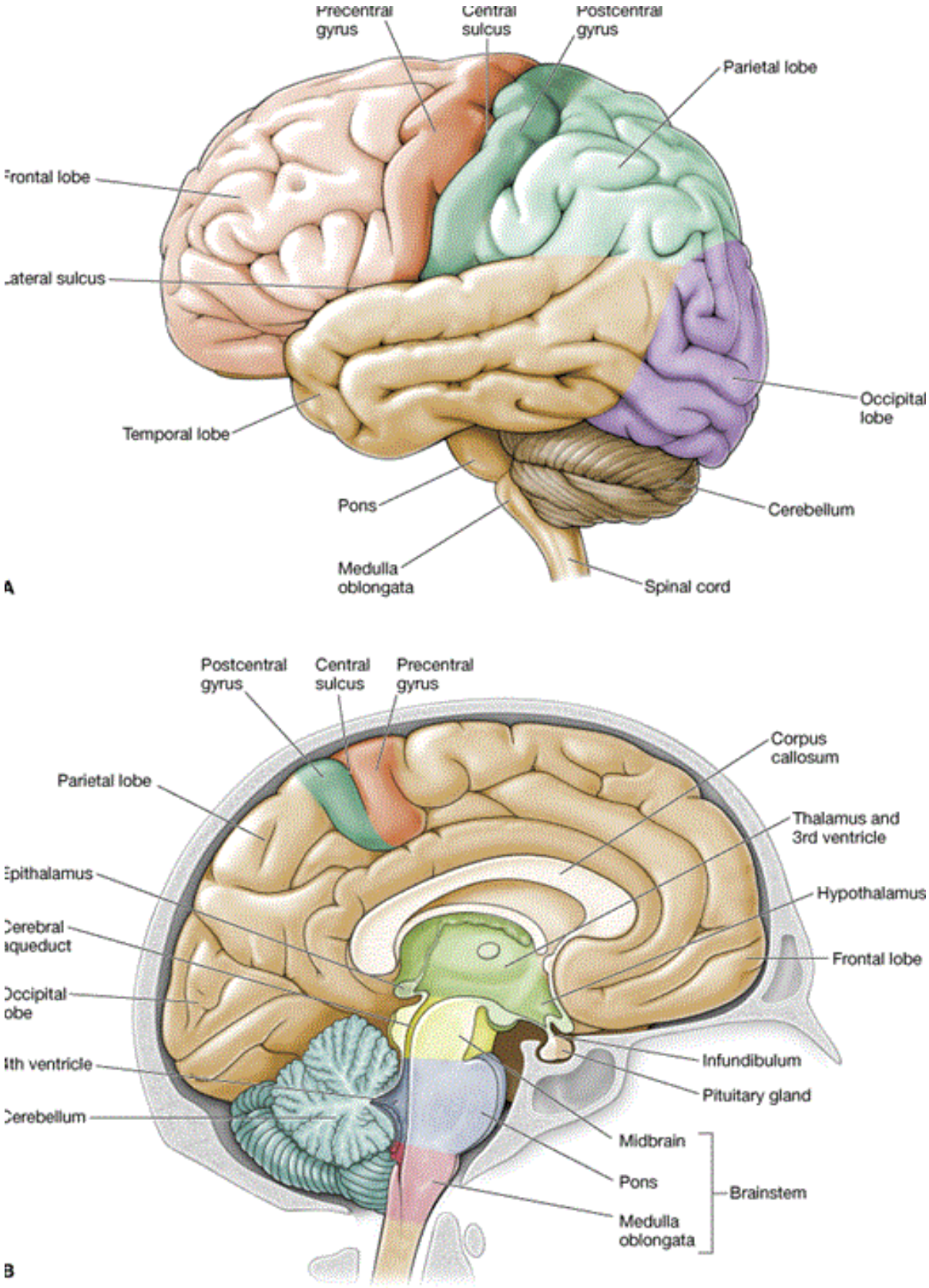

Figure 1. Sagittal sections of the brain. A: Lateral View of the Brain; B: Midsagittal (Medial) View of the Brain. Morton DA, Foreman KB, Albertine KH: The Big Picture: Gross Anatomy.

The cerebrum is made up of two almost symmetrical structures, separated by a deep longitudinal fissure, which are called the right cerebral hemisphere and the left cerebral hemisphere. Each hemisphere is specifically adapted for some functions with respect to the other: this functional specialization is called lateralization. There can be identified 4 lobes on each cerebral hemisphere, shown in Figure 2. The frontal lobe is the emotional control center of the brain, responsible of the formation of the personality, decision making and regulation of social behaviour. It is located in rostral position with respect to the central sulcus, where it receives information signals from other lobes of the brain. It is responsible for problem solving, judgement and motor function, it also controls thinking, planning, organizing, short-term memory and movement, due to the presence of the primary motor cortex [1]. The parietal lobe processes information for cognitive purposes and helps coordinate spatial relations. It is located in the middle section of the brain in rostral position with respect to the occipital lobe, but caudal with respect to the frontal lobe and the central sulcus. It is responsible for the management of sensations, body position and handwriting. It processes sensory information from different parts of the body, as well as temperature and touch [1]. Some functions of the parietal lobe include sensing pain, pressure, touch, regulating and processing the body's five senses, movement and visual orientation, speech, visual perception and recognition, cognition and information processing [2]. The temporal lobe is located underneath the lateral sulcus, there is one temporal lobe on each side of the brain, in proximity of the ears. This lobe is where the primary auditory cortex resides, that is important to interpret the sound and language heard by the individual. In addition to their primary function of processing auditory stimuli, the temporal lobes are also involved in memory storage, hearing, processing information from the senses of smell and taste [1]. Some functions of the parietal lobe include help in the formation of long-term memory, processing new information, formation of visual and verbal memories, interpretation of smell and sounds [2].

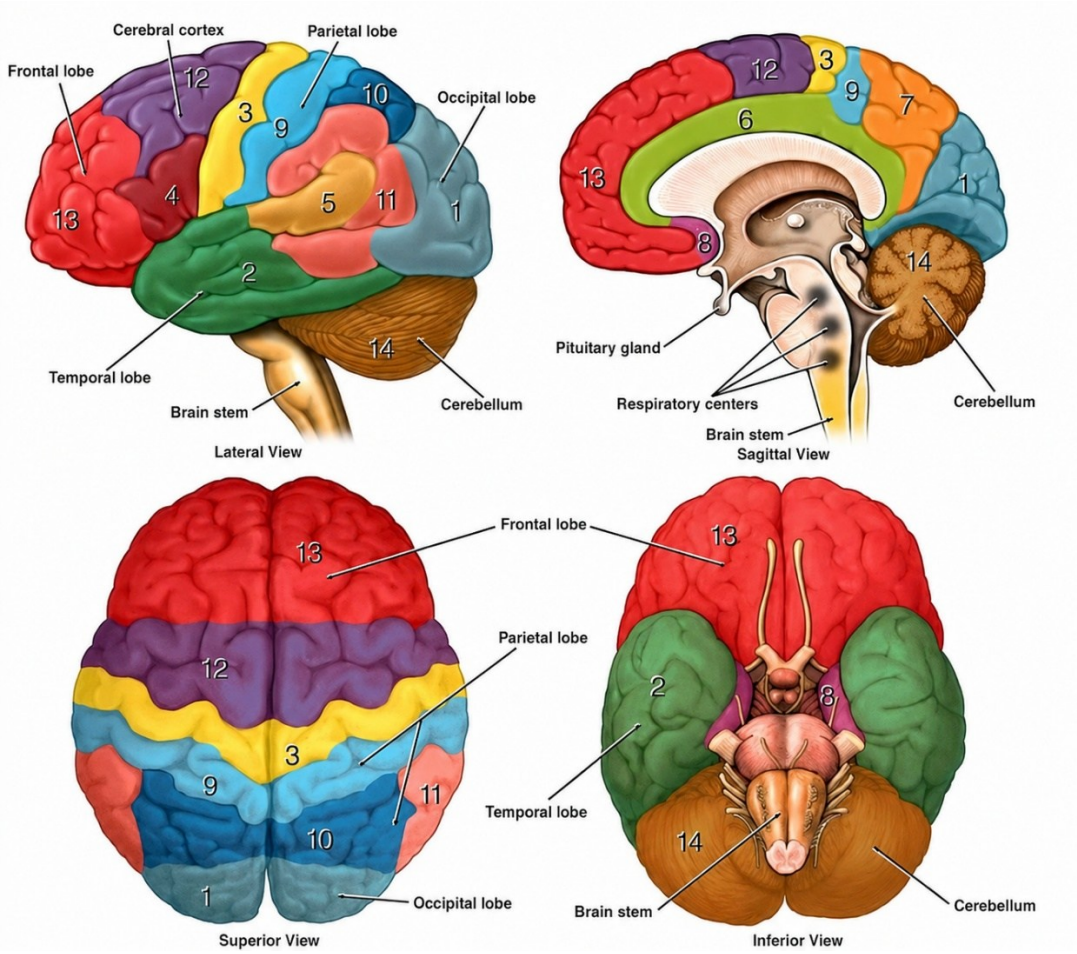

1 Visual Area:
Sight
Image recognition
Image perception

2 Association Area
Short-term memory
Equilibrium
Emotion

3 Motor Function Area
Initiation of voluntary muscles

4 Broca's Area
Muscles of speech

5 Auditory Area
Hearing

6 Emotional Area
Pain
Hunger
"Fight or flight" response

7 Sensory Association Area

8 Olfactory Area
Smelling

9 Sensory Area
Sensation from muscles and skin

10 Somatosensory Association Area
Evaluation of weight, texture, temperature, etc. for object recognition

11 Wernicke's Area
Written and spoken language comprehension

12 Motor Function Area
Eye movement and orientation

13 Higher Mental Functions
Concentration
Planning
Judgment
Emotional expression
Creativity
Inhibition

Functional Areas of the Cerebellum

14 Motor Functions
Coordination of movement
Balance and equilibrium
Posture

Figure 2. Brain anatomy and functional areas.

The occipital lobe is located in the posterior portion of the brain, in caudal position with respect to parietal and temporal lobes. It contains the primary visual cortex and the visual association cortex; it processes visual information form the eyes and links that information with images stored in memory [1]. Other functions of the occipital lobe are visual-spatial processing, as well as movement and color recognition [2].

Korbinian Brodmann was a German neurologist who made a fundamental contribution to neuroscience through his cytoarchitectonic classification of the cerebral cortex. In the early 20th century, he subdivided the human cerebral cortex into 52 distinct regions based on their histological structure and cellular organization. This classification, now known as Brodmann areas, is based on the observation that the cerebral cortex is composed of six cellular layers shown in Figure 3, whose structure and arrangement vary across different regions. Each area identified by Brodmann is characterized by a specific organization of these layers and of the constituent cells. Importantly, these structural differences are associated with functional specialization, allowing each region to be linked to particular brain functions. Brodmann assigned a numerical label to each area, and this nomenclature is still widely used in modern neuroscience to refer to specific cortical regions [4].

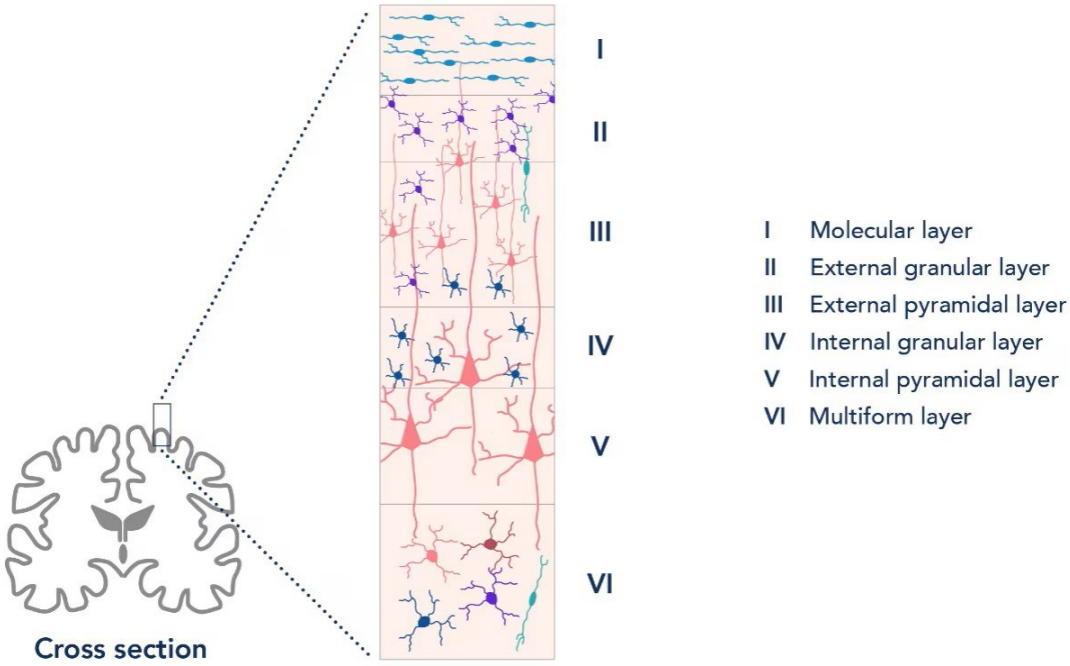

Figure 3. The six cellular layers of the cerebral cortex. From Heimer 1994.

Brain connectivity refers to functionally specialized brain regions interacting with each other rather than operating as isolated units, so different cortical areas communicate and cooperate to support complex brain functions. Brain connectivity can be classified into three main types: structural connectivity, functional connectivity and effective connectivity. The structural connectivity refers to the physical connections between brain regions. These connections are formed by synaptic links between neurons or by white matter fiber tracts that connect distant areas of the brain. The complete set of these connections constitutes the connectome. Functional connectivity is defined as the temporal correlation between neuronal activation patterns in spatially distinct brain regions. It reflects statistical dependencies between different areas that may be involved in similar or related processes. These interactions are often associated with synchronized neural activity. Effective connectivity describes the causal influence that one brain region exerts over another. Unlike functional connectivity, it accounts for directionality and attempts to model the underlying mechanisms of interaction within neural systems [4]. A compact representation of brain connectivity is made possible through the use of a connectivity matrix, where each element corresponds to the strength of the connection between two regions. These matrices are often visualized using colormaps, which allow an immediate interpretation of connectivity patterns [4].

1.1.2 Cerebral Electrophysiology

The basic elements of the nervous system are the glial, or neuroglia cells, and the neurons. The glial cells outnumber neurons by a ratio of approximately 3 to 1 in the human brain. Glial cells do not directly participate in synaptic transmission or electrical signaling. Instead, they perform essential supportive functions [2]. Among their most important roles is the production of myelin, a lipid-rich insulating sheath that wraps around axons and significantly increases the speed of action potential propagation. Neurons are the fundamental signaling units of the nervous system, specialized for the reception, integration, and transmission of information. From a morphological point of view, the neuron can be compared to a tree, having three main elements: the cell body, the axon and the dendrites, as shown in Figure 4. Cell body, or soma, contains the nucleus, where the DNA of the neuron lies. The axon is the output structure that transmits electrical messages to other neurons, muscles, or glands. In many neurons, the axon is surrounded by a myelin sheath, formed by oligodendrocytes in the central nervous system and Schwann cells in the peripheral nervous system. This sheath is not continuous; it is interrupted at regular intervals by gaps called nodes of Ranvier. As will be described in detail later, this specialized structure enables saltatory conduction, dramatically increasing the velocity of action potential propagation. The dendrites are input structures that receive electrical signals from axons of other neurons and convey them toward the soma. The electrical event

by which neurons convey signals, and therefore information, is the action potential. The action potential is a self-regenerating electric wave that propagates from its point of origin in the cell body to the end of the axon, where connections with other neurons are formed. Cells have a system capable of generating a constant potential difference between the two faces of their membrane when it is at rest: this is called the resting membrane potential or the resting potential. The action potential modifies the negative resting potential and makes the transmembrane potential temporarily positive. Despite the cells of our body present a great morphological and functional variety, they have some features in common, such as the cell membrane. It has two functions: separate the intracellular compartment from the extracellular one and selectively connect the two environments. The cell membrane has a thickness of 7.5-10 nm and is composed mainly of proteins and lipids. It consists of a phospholipid bilayer that extends continuously over the entire cell surface [1].

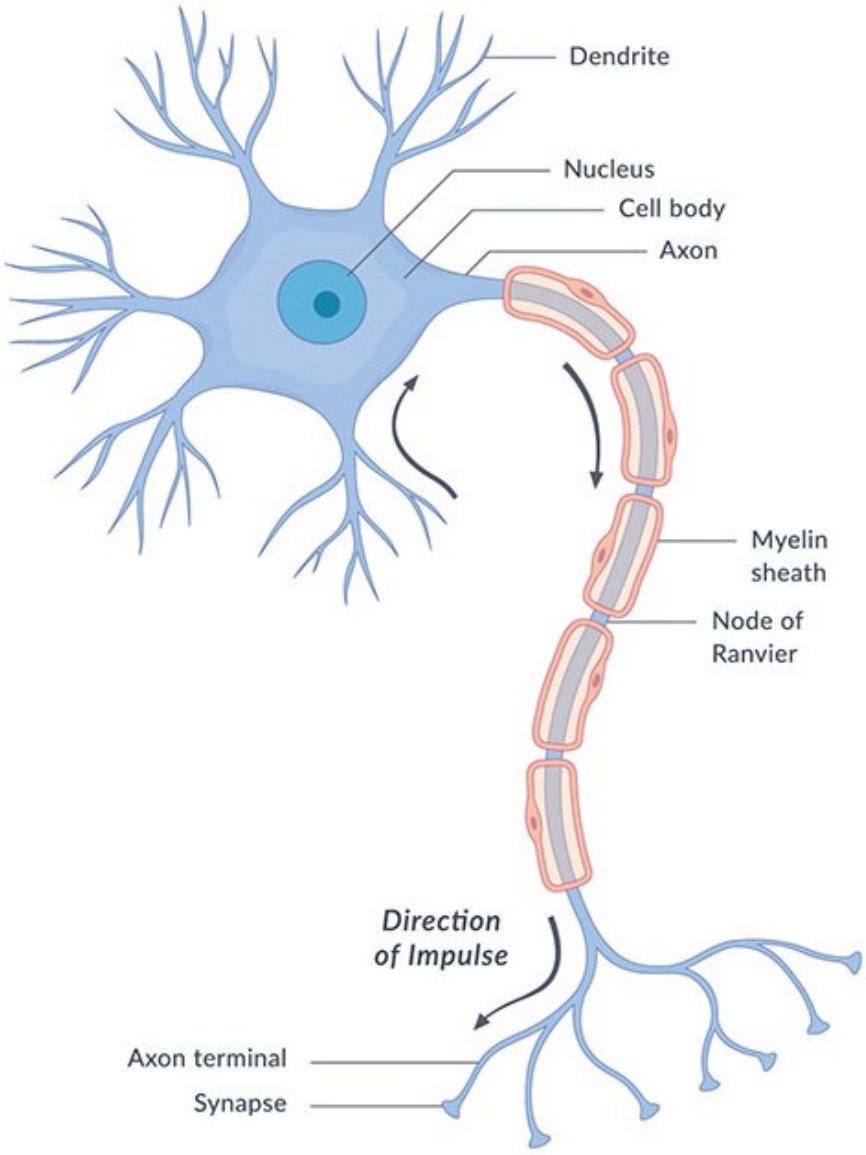

Figure 4. Structure of a neuron.

Phospholipids are molecules that have a head and a tail. In water solution, phospholipids arrange themselves in bilayers, with hydrophobic tails in the center and hydrophilic heads on the outside. The membrane results almost completely impermeable to water and other water-soluble substances, as ions and glucose, commonly present in the cell, while is permeable to liposoluble substances, such as oxygen, carbon dioxide and alcohols. In the phospholipid films there are interposed large molecules of transmembrane proteins which constitute the structural crossing means of the membrane, called pores, through which water and ions can diffuse between the intracellular and extracellular liquid. Is important that pores have selective properties in order to allow a preferential diffusion of certain substances rather than others and determine the semi-permeability of the cell membrane. Proteins and glycoproteins that pass through the cell membrane or are attached to it allow the cell to carry out its metabolic and transport activities, as well as the electrical activity. In particular, the electrical activity of the cell is due to ions flowing across the cell membrane, the most important being sodium (Na^+), potassium (K^+), chlorine (Cl^-) and calcium (Ca^{2+}) [3]. These ions can pass from the inside of the cell to the outside and vice versa through two mechanisms: diffusion (which is a naturally occurring phenomenon and does not require the cell to exert any of its energy to accomplish the transport, since ions move from an area of higher concentration to an area of lower concentration) and active transport (which requires the cell to spend energy to accomplish the transport, since ions move from an area of lower concentration to an area of higher concentration). The ions, present in variable concentrations in the interstitial fluid and inside the cell, create an ionic current across the membrane determined essentially by two diffusion mechanisms: the free diffusion and the ionic diffusion. In the first case the movement is guided by the mass concentration, in the second case the movement is guided by the electric field in which the ions are. This ionic separation, occurring at the cell membrane, creates a chemical gradient across the membrane. Because ions are charged particles, we also need to consider their charge when thinking about their distribution across the membrane. At rest there are more positively charged ions outside the cell relative to the inside. This creates a difference in charge across the membrane, which is called electrical gradient. Thus, we refer to this ionic imbalance as the electrochemical gradient [3]. The difference in total charge inside and outside of the cell is the membrane potential. For each ion the electrical gradient and chemical gradient are equal and opposite. The ions can move from one side to another of the membrane thanks to proteins embedded in the membrane, which act as ion channels. The flowing of ions across the cell membrane involves the creation of ionic currents that are important for the electrical activity of the cell. The differences in the concentration of ions across the membrane determine a difference in potential at rest called transmembrane potential. The free diffusion due to the different concentration of ions in the intra and extracellular environment causes the movement of ions across the cell membrane. This means a small

change of polarity across the membrane. As a consequence of the free diffusion, the ions gather at the edges of the cell membrane, and this creates a potential difference and an associated electric field. Indeed, the change of polarity, although small, combined with the small thickness of the membrane, can determine a significant electric field. Indeed, the electric field exerts a force on the ions, influencing their movement. Thus, any description of the ion flux across the membrane has to consider both the free diffusion and the ionic diffusion. The equilibrium is reached when the ion flux due to free diffusion is equal to the ion flux due to ionic diffusion. At rest, the Cl^- ion is usually very close to equilibrium, while K+ and Na+ are not. This is due to the presence in the cell membrane of the sodium-potassium pump, which represents a mechanism of active transport of ions. The sodium-potassium pump allows a dynamic balance to be maintained at the expense of cellular metabolism [1]. Through the sodium-potassium pump the ionic concentrations between inside and outside remain the same, regardless of the passive equilibrium currents. So, a high concentration of K+ ions is maintained inside the cell, and of Na+ outside. As previously mentioned, the membrane potential measures the potential difference between the inside and outside of the cell, which is about -60/-75 mV for an unstimulated neuron [3]. If the neuron is stimulated and the resulting change in membrane potential remains below the threshold required to trigger an action potential, this is referred to as a graded potential. Graded potentials can vary in size, can be either positive or negative, are transient and typically do not result from the opening of voltage-gated ion channels. When a graded potential occurs, the neuron resets its membrane potential to resting values. This is performed primarily by the sodium-potassium pump, which exploits the energy generated by ATP hydrolysis to actively transport ions across the membrane against gradient: sodium is transported to the outside of the cell and potassium is transported back into the cell, where their concentrations are higher. All this contributes to keep the resting ionic levels, restoring the electrochemical gradient. The maintenance of this balance is important for neurons. Indeed, this process can account for 20% to 40% of the brain total energy use. When the outside stimulation is large enough to bring the membrane potential in the neuron body up from -70 mV to the threshold voltage of - 55 mV, or higher, an action potential arises [3]. The voltage-gated sodium channels have three states: open, closed, and inactivated. At rest, the sodium channel is closed. The moving of cell membrane from its state of resting implies that the channel changes to an open position and sodium starts to enter the cell following the electrochemical gradient. When the cell membrane reaches the threshold voltage, this phenomenon becomes more intense. Since sodium ions are positive, the membrane potential becomes less negative and more positive as it approaches 0 mV, this process is called depolarization. Then, the voltage gradient reaches a positive value around 30 mV, this is called overshot. When the membrane potential becomes positive, the sodium channel inactivation gate closes, making the channel inactivated and the flow of

sodium ions into the cell stops. The changing membrane potential also opens the voltage-gated potassium channels and potassium ions flow out of the cell. The membrane potential becomes less positive and then negative, this process is called repolarization. Since the potassium channels are a little slow to close, for a brief period, the membrane potential is hyperpolarized. Throughout these phases, the sodium-potassium pump is still working. The pump acts to restore the chemical gradients by moving more sodium ions out than potassium ions in and restore the cell membrane resting potential. During repolarization, the inactivated sodium channels will not respond to any stimulus, no matter how strong it is, and the neuron is said to be in its absolute refractory period. The absolute refractory period prevents action potentials from arising again too quickly and prevents action potential from travelling backwords along the axon. Instead, the hyperpolarization period is also called relative refractory period. In this period the sodium channels are closed, and the inactivation gate opens. This means that sodium channels could open, but it would take a larger than usual stimulus to reach threshold. The action potential, Figure 5, has a duration of about 1-2 ms and an amplitude of about 100-120 mV and it never changes, so it does not get bigger with a bigger stimulus [3]. However, it is important to note that action potential morphology (including duration, amplitude, and shape) varies considerably across different cell types. For example, cardiac myocytes exhibit action potentials lasting hundreds of milliseconds, while some interneurons display action potentials with durations of less than 0.5 ms. An action potential occurs when the membrane depolarizes to a certain threshold: if this threshold is not reached the action potential will not be triggered and if the threshold is exceeded, the action potential does not get bigger. This is referred to as the all-or-nothing principle in biology: it means that the power of a stimulus is not proportional to the power of the action potential. Moreover, any suprathreshold stimulus will produce an action potential of similar amplitude and duration within a given neuron.

In myelinated fibres the conduction of the action potential does not occur in a continuous manner but with a saltatory mechanism, resulting in an increase of the speed of conduction. The action potential signal seems to jump along the part of the processes covered by the sheath. The parts that are not covered by myelin are called nodes of Ranvier and the action potential appears to jump from node to node, speeding the transmission [2]. Then, the positive charge that has triggered the action potential in one region will move to the adjacent region of the membrane, causing the adjacent region of the membrane to depolarize. If it depolarizes enough, a new action potential will be triggered. This happens in cascade region after region. The presence of myelin cancels the sodium channels so that the action potential cannot propagate actively. This means that the potential change produced by the action potential at one node of Ranvier propagates in the myelinated region along the axon passively.

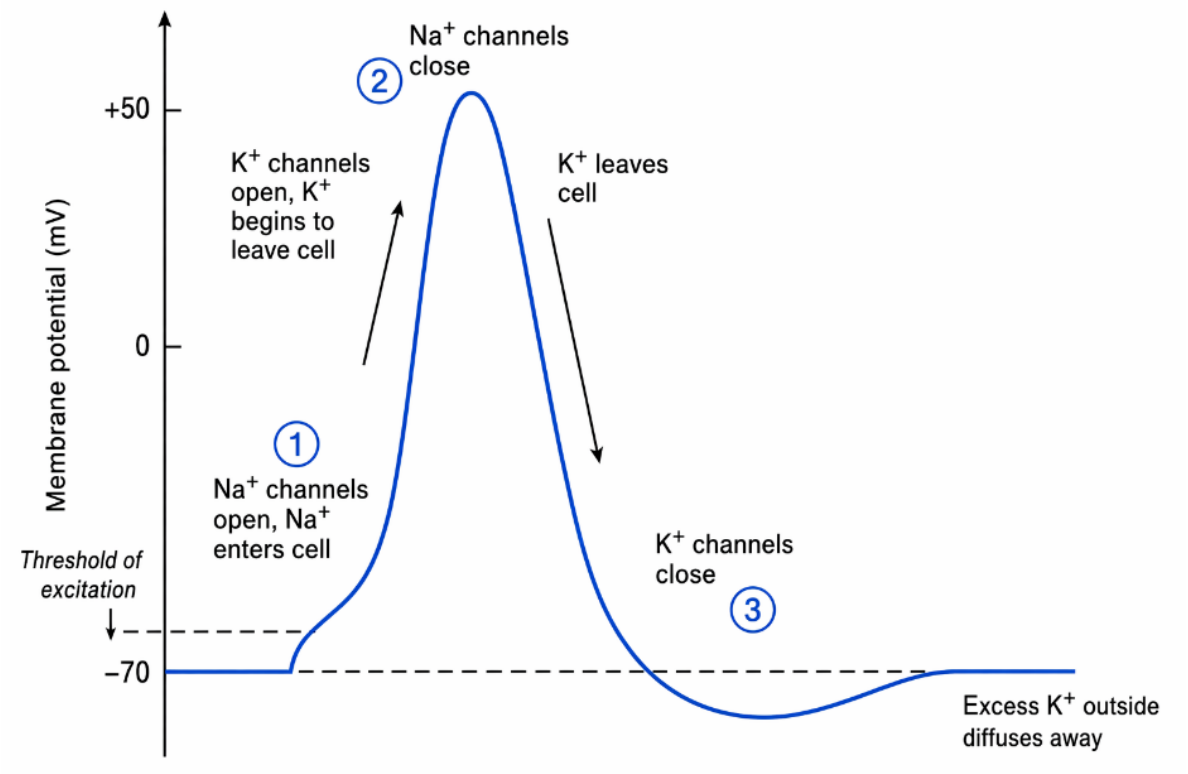

Figure 5. Graph of an action potential.

The potential passively propagated becomes smaller in intensity, but in correspondence of the next node, a new action potential will be triggered. The change in the membrane potential, because of this action potential, is the depolarization that comes from the end of the myelin sheath. Therefore, each node acts as a relay station that renews the small potential. Communication between neurons is made possible by synapses, they are functional contacts between neurons. The mechanism of communication between neurons is twofold, so two categories of synapses can be distinguished: electrical synapses and chemical synapses. In electrical synapses, the membranes of the two communicating neurons are in intimate contact at the synapse and are held together by a specialized intercellular structure called gap junction [1]. Gap junctions consist of exactly aligned pairs of channels in the membrane of the presynaptic and postsynaptic neuron so that each pair of channels forms a pore. Electrical synapses work in a way that allows ionic currents to flow from one neuron to another through these pores. The source of this current is the potential difference generated locally by the action potential. Transmission can occur bidirectionally, the direction of propagation depends on which neuron the action potential passes through. The electrical synapse allows for practically instantaneous transmission. A more general function of electrical synapses is to synchronize electrical activity between various populations of neurons. In a chemical synapse, the gap between the presynaptic neuron and the postsynaptic neuron is greater than that of an electrical synapse and is called the synaptic cleft. Inside the synaptic terminal there are small organelles called synaptic

vesicles. These spherical organelles contain one or more neurotransmitters, the chemical signals secreted by the presynaptic neuron. The communication process begins when an action potential reaches the synaptic termination of the presynaptic neuron. The change in membrane potential caused by the arrival of the action potential causes the opening of voltage-gated calcium channels in the presynaptic membrane. Because of the high concentration of calcium ions in the external environment, they enter the synaptic termination of the presynaptic neuron, leading to the fusion of the synaptic vesicles with the plasma membrane of the presynaptic neuron [2]. Consequently, their contents are released into the synaptic cleft, thus the neurotransmitters bind to specific receptors located on the membrane of the postsynaptic neuron, causing certain channels in the postsynaptic membrane to open or close, changing the flow of ions across them. The resulting neurotransmitter-induced current flow changes the membrane potential of the postsynaptic neuron, increasing or decreasing the likelihood that the neuron will fire an action potential. In some cases, postsynaptic potentials increase the probability of occurrence of a postsynaptic action potential and are therefore called excitatory. In other cases, postsynaptic potentials decrease the probability of occurrence of a postsynaptic action potential and are then termed inhibitory [2]. The postsynaptic potential is either excitatory or inhibitory depending on the type of channel that is coupled to the receptor and the concentration of ions inside and outside the cell. An excitatory postsynaptic potential determines an action potential more positive than the threshold value necessary for the trigger, meaning that it tends to depolarize the membrane potential leading it to exceed the threshold value. An inhibitory postsynaptic potential causes an action potential more negative than the threshold, so it tends to hyperpolarize the membrane potential or to keep it at its resting level. Excitatory postsynaptic potentials depolarize the postsynaptic cell, while inhibitory postsynaptic potentials can either hyperpolarize or depolarize it. The level of excitatory postsynaptic potentials produced by the activity of individual synapses is often well below that required to trigger a postsynaptic action potential. Neurons in the central nervous system are innervated by thousands of synapses, and postsynaptic potentials can sum, over time and space, to determine whether a postsynaptic action potential will be generated. Summation allows subthreshold postsynaptic potentials to influence the generation of an action potential. The summation of excitatory and inhibitory postsynaptic potentials allows the postsynaptic neuron to integrate the electrical information provided by all inhibitory and excitatory synapses. The possibility that the summation of active synaptic stimuli determines the generation of an action potential depends on the balance between excitation and inhibition. If the summation results in a depolarization of sufficient magnitude to drive the membrane potential of the postsynaptic neuron above threshold, then the postsynaptic neuron will produce an action potential, otherwise the neuron will remain silent. The balance between excitation and inhibition changes continuously over time as

a function of the number of excitatory and inhibitory synapses that are active at a given moment, as well as a function of the intensity of the stimulus at each synapse.

1.2. ELECTROENCEPHALOGRAM

One of the most effective tools for studying brain activity is electroencephalography (EEG), which measures electrical signals generated by the brain through electrodes placed on the scalp. EEG recordings are commonly analyzed by examining the spectral power of different brainwave frequencies, providing insight into motor-related processes such as movement execution and motor imagery.

1.2.1 Acquisition Modalities and signal description

The electrical activity of the brain can be recorded directly in two ways: surface electroencephalography, which is a non-invasive procedure, since the acquisition takes place at the level of the scalp; and electrocorticogram, which is an invasive procedure, since the acquisition takes place at the level of the cortex. For the purpose of this thesis, we will focus on the first one. The most numerous cells in the cortex are the pyramidal cells, called this way because of their conic shaped soma. Pyramidal cells are neurons with a single axon, a large apical dendrite, multiple basal dendrites, and dendritic spines. They are the main neuronal source of EEG. There are two main types of electrical activity associated with pyramidal neurons: action potentials and post-synaptic potentials. Action potentials do not contribute to the EEG signals. Surface electrodes cannot generally detect action potentials due to their timing and the physical arrangement of the axons. First, action potentials have a very short duration (approximately 1 ms), making them difficult to capture. Second, and more importantly, the axons of cortical neurons are not uniformly oriented: they project in various directions, and the electric fields generated by action potentials propagating along differently oriented axons tend to cancel each other out. Furthermore, most axons are located in the subcortical white matter, far from the scalp surface, and the signal amplitude decreases significantly with distance. As a result, the contributions of action potentials to the EEG signal are minimal and are typically lost in the background activity. It is impossible to detect single action potential, while the signal would be stronger and detectable if action potentials sum. Thus, action potentials would only be recorded if neurons fire at the same time and have axons oriented in the same direction: in this case, the voltages of the action potentials sum. However, neurons rarely fire at the same time and axons are relatively random oriented, thus they generally cancel each other out. Therefore, action potentials are lost in the background activity and contribute little to the signals recorded by scalp electrodes. Postsynaptic potentials arise when neurotransmitters bind to receptors on the membrane of the post synaptic cell,

causing ion channels to open or close and leading to a change in potential across the cell membrane. Differently from action potentials, postsynaptic potentials are longer in duration than action potentials, lasting up to tens or hundreds of milliseconds. They are generally present in the dendrites of a neuron. Since dendrites are oriented in parallel, they can sum and are considered to largely contribute to the signal measured by EEG. The cell bodies of pyramidal neurons are located in cortical layers and are arranged parallel to each other and perpendicular to the surface of the cortex. Their dendrites extend to the more superficial cortical layers as showed in Figure 5. The activation of dendrites that produce excitation or inhibition can be synchronized and produce electrical potentials between the proximal and distal regions of a dendrite. The excitatory inputs are mostly found in the distal regions of the dendrite while the inhibitory inputs are closer to the cell body. This relative anatomical separation between excitation and inhibition allows for the existence of an electric dipole. When large numbers of neurons are synchronous (meaning they generate postsynaptic potentials at the same time) the net effect of excitatory and inhibitory postsynaptic potentials are summed together and can be perceived as signal from an electrode on the scalp. So, EEG signals are potentials that arise from the synchronized synaptic activity of pyramidal neurons, which are organized in columns perpendicular to the cortical surface [4]. The scalp electrodes record the summated electrical activity generated by thousands of synchronously active pyramidal neurons. The resulting signal magnitude is proportional to the number of neurons involved, as well as their spatial alignment and distance from the recording electrode. Surface EEG measures the activity of cortical neurons located just below the scalp, and thus, the electrical contribution of deeper structures, such as thalamus, hippocampus, or brainstem, is minimal and can simply modulate the EEG signals. After they are generated, EEG signals travel from the cortex, through the meninges, the skull, and the scalp to reach the electrodes, as showed in Figure 6. The voltage measured at the scalp fluctuates between positive and negative values at a rate that defines the frequency of the signal. For an excitatory postsynaptic potential, the depolarization of the dendritic membrane causes an influx of positive charges into the cell, leaving a negative extracellular charge where the synapse is located. In turn, compensatory return currents are determined: this causes a positive extracellular charge at a distance along the dendritic membrane. For an inhibitory postsynaptic potential, the hyperpolarization of the dendritic membrane causes an influx of negative charges into the cell, leaving a positive extracellular charge where the synapse is located. In turn, compensatory return currents are determined: this causes a negative extracellular charge at a distance along the dendritic membrane. Therefore, excitatory post-synaptic potentials (EPSP) cause extracellular negativity at the synapse, the active sink, due to the influx of Na+ ions and extracellular positivity at the passive source, due to the compensatory current. Instead, inhibitory post-synaptic potentials (IPSP) cause extracellular positivity, the active source, due to the influx of

Cl- efflux of K+ ions, and extracellular negativity at the passive sink, due to the compensatory currents [5].

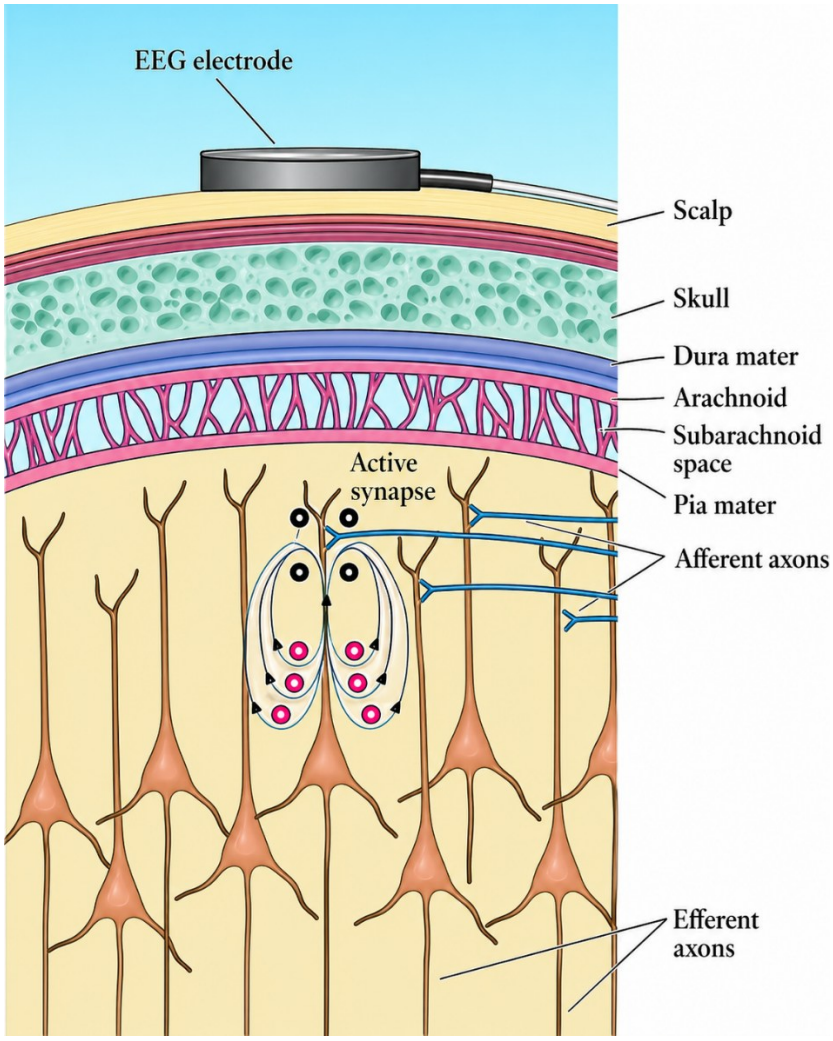

Figure 6. The figure illustrates the pyramidal cells and how the electrical signal travels to the scalp electrodes [4].

The position and orientation of the cortical area generating the EEG signal determines the distribution of the negative and positive potentials on the scalp. Cortical sources can have radial and tangential orientation with respect to the cortical surface: radial sources are typically found on the cortical convexity (the gyral crowns) and in this case, the apical dendrites of pyramidal neurons are oriented perpendicular to the cortical surface, and the electrical dipole points towards the scalp. The return currents flow deep into the cortex, creating a potential difference that is clearly detected by scalp electrodes. This configuration generates strong EEG signals. While the tangential sources are found in the walls of sulci where the apical dendrites are oriented parallel to the cortical surface, and the dipole points horizontally. The return currents are also parallel to the surface, meaning that the positive and negative fields are distributed laterally rather than vertically. As a result, the potential

difference at the scalp is minimal, making tangential sources more difficult to be detected with standard EEG recordings [5]. EEG is acquired through surface electrodes, that are conducting devices applied at different positions of the scalp, made of non-polarized material to avoid signal instability. There are mainly three types of electrodes: gel, dry and water electrodes. The gel electrodes are the most widely used type of electrodes, they have been the gold standard in EEG research for a long time. The electrode is commonly made of silver with a coating of silver chloride (Ag/AgCl) [6]. A gel containing many chloride ions is applied between the skin and the electrode to improve conduction and reduce the skin-electrode interface impedance. Therefore, the gel between the skin and electrode allows for good-quality recording of biopotentials. The preparation time of a gel EEG cap requires time as the skin needs to be abrased by a trained technician. This type of electrodes allows for high-density EEG recordings, high signal quality, stable recordings for a long time, it is also less sensitive to interference and movement artifacts with respect to water and dry electrodes. On the other hand, some disadvantages carried by this type of electrodes are: the skin needs to be prepared by lightly scratching the skin to reduce impedance; they are inconvenient for researchers because the preparation time can be long, the head cap requires cleaning, also drying of the cap takes time; they are inconvenient for participants since hair needs to be cleaned and scratching the skin can feel uncomfortable; they require a skilled technician; the conductive gel can dry out over time during recordings over 5 hours [6]. Dry electrodes were proposed as an alternative to overcome the common issues with wet electrodes. Dry EEG electrodes consist of an inert conductive material that mechanically couples with the skin for signal transduction and eliminates the need for gel or skin preparation [7]. Dry electrodes are composed using various materials and shapes. Since dry electrodes do not use a conductive gel or abrasive paste, there is a higher electrode impedance seen with dry electrodes than with wet electrodes [7]. Also, this can lead to poor contact noise, increased signal instability, and more sensitivity to movement artifacts. Resuming, they require quicker setup time than gel electrodes, they do not require skin preparation, they are suitable for at-home testing, in addition they need almost no clean-up, and, on some occasions, it is possible to use them without a trained technician. However, they present a higher difficulty in keeping electrodes in fixed contact with the skin, an increased signal instability and higher impedances. Moreover, they show a higher susceptibility to interference and movement artifacts than gel electrodes, but limited actions are possible to improve the skin-electrode contact quality, they are also quite uncomfortable to the wearer due to the need for a stable mechanical coupling; since no gel is used to cushion the contact, the electrodes must be pushed against the scalp with force to lower impedance, which creates pressure points and makes them particularly uncomfortable over extended sessions. Water electrodes, also called semi-dry electrodes, like dry electrodes, have a short preparation time and do not require the

use of a conductive gel. The key feature of water electrodes is that they use water or an electrolyte liquid. Some water electrodes use water sponges with tap water or saline water to increase the conduction between the skin surface and the electrode [7]. Other water electrodes slowly and continuously release a tiny amount of electrolyte liquid to the scalp in a controlled fashion. Since these methods do not require the application of gel or abrasion of the skin, they also have a faster preparation time and clean-up than gel electrodes. Some advantages of water electrodes are: quicker setup and clean-up time than gel electrodes; they are suitable for at-home testing; it is possible to use them without a trained technician in some situations; they also overcome problems with high impedance and signal instability seen in dry electrodes with water. Instead, some disadvantages are: they dry out quicker compared to gel electrodes, so they need to be remoistened more often; they are more susceptible to mains interference and movement artifacts than gel electrodes, but limited actions are possible to improve the skin-electrode contact quality. Table 1 provides a comprehensive comparison of the three electrode types across the key features discussed above.

Table 1. Comparison between gel, dry, and water EEG electrodes

Feature	**Gel Electrodes**	**Dry Electrodes**	**Water Electrodes**
Materials used	Ag/AgCl with gel reservoir	Inert conductive materials	Conductive material with water or electrolyte liquid
Skin preparation	Required (abrasion)	Not required	Not required
Setup time	Long	Quick	Quick
Need for trained technician	Yes	Usually not	Sometimes not
Skin-electrode impedance	Low	High	Moderate
Signal quality	High	Lower	Good
Signal stability	Stable over long recordings	Unstable	Better than dry
Susceptibility to movement artifacts	Low	High	Moderate
Comfort for the participant	Moderate	Low	Moderate
Suitability for long recordings	Good (but gel may dry out)	Good	Limited (needs remoistening)
Suitability for at-home testing	No	Yes	Yes

The choice of electrode type depends on multiple factors, including desired signal quality, time constraints, availability of a trained technician, and mobility. In any case the electrode should not significantly attenuate signals between 0.5 Hz and 70 Hz. Its impedance depends on the electrical resistance of the skin and the contact between the skin and the electrolytic paste. The electrode impedance should not be too high not to cause noise artifacts, nor too low in order to have a detectable signal. The skin has to be prepared before the application of the electrodes, to eliminate dirt and oil that could reduce the impedance. Throughout the acquisition a good electrode/skin contact should be maintained.

In clinical application, scalp electrodes are placed at standard positions, following the guidelines of the International Federation of Clinical Neurophysiology (IFCN). The standard IFCN array is an

extension of the so-called international 10–20 system [8]. The standard implies the positioning of the electrodes according to fundamental ideal lines drawn starting from fixed landmarks: the inion, the external prominence of the occipital bone; the nasion, the small depression immediately above the nose; and the preauricular points. The distance between one electrode and another is 10% or 20% of the total length of the line, hence the name of the system. The first measurement that is made is from the nasion to the inion. The measurement is then divided into 10% or 20% intervals and marks are placed. Then, a measurement is made from one preauricular point to the other. Analogously, this length is divided in 10% or 20% intervals and marks are placed, as showed in Figure 7. Further marks are made around the circumference of the head at intervals of 10%. Further measurements are made in the sagittal and transverse plane, considering 25% intervals and marks are placed [8]. According to the international 10–20 system, the position of each electrode is labelled according to the lobe (Figure 8), or more in general the area of the brain, in which the electrode is placed: prefrontal (Fp), frontal (F), temporal (T), parietal (P), occipital (O), and central (C). Electrodes are also numbered according to the side of placement: even numbered ones are those placed on the right hemisphere, while odd numbered ones are those placed on the left hemisphere.

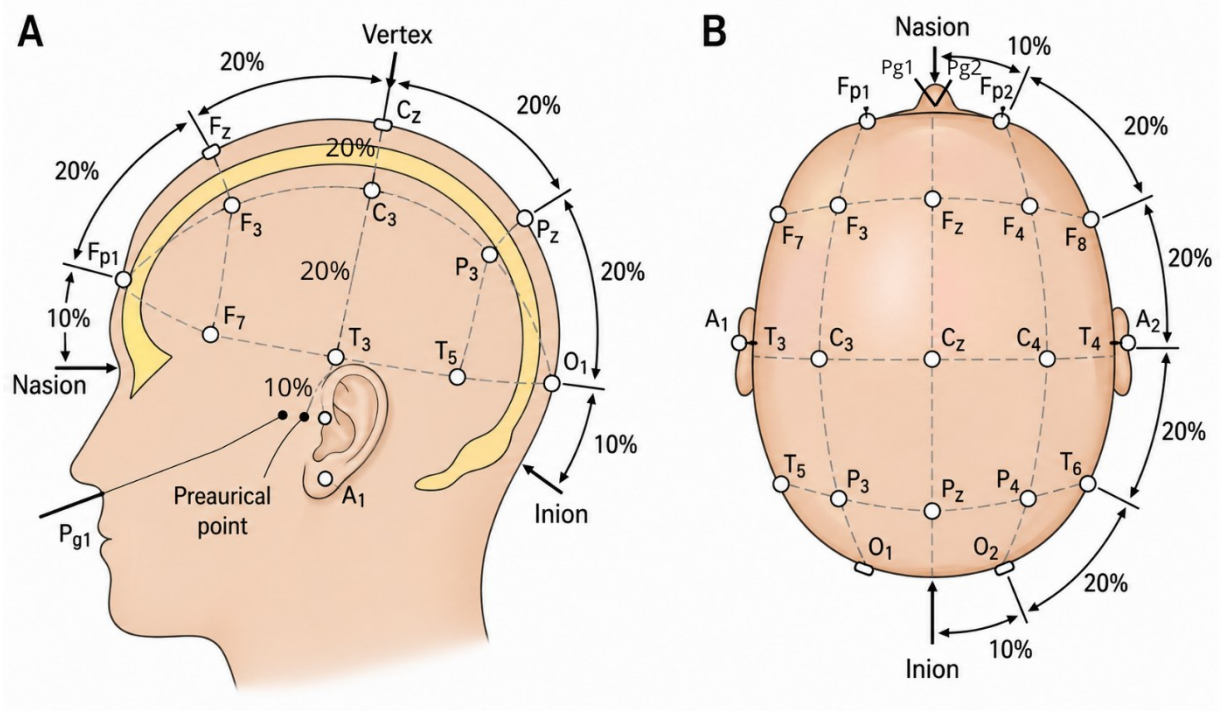

Figure 7. The International 10-20 System seen from the sagittal (A) and horizontal (B) planes. A, ear lobe; C, central; F, frontal; FP, frontal polar; O, occipital; P, parietal; Pg, nasopharyngeal [8].

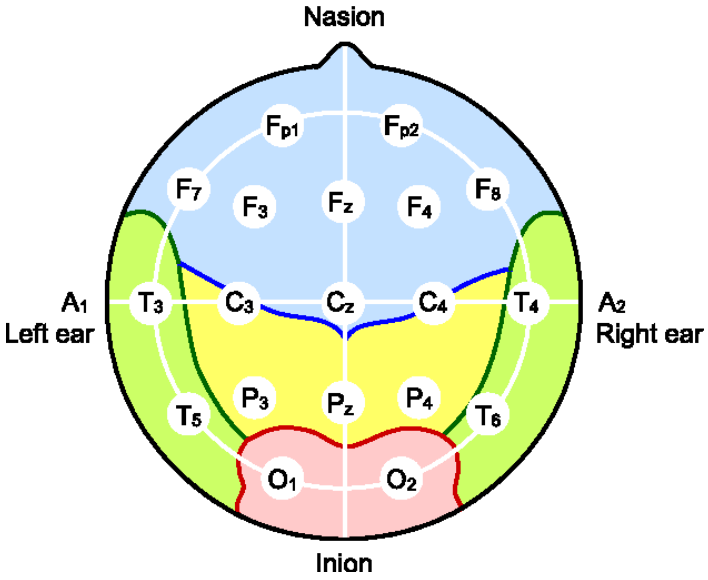

Figure 8. 10-20 system electrodes placement [9].

Electrodes with lower numbers are closer to the midline and electrodes with higher numbers are farther away from the midline. Electrodes with Z in the label are those placed in the middle sagittal plane [9]. Besides the scalp EEG electrodes, one or more ground electrodes are placed and connected to the jack box of the EEG recorder and their positions are specified by the manufacturer. Higher density electrode systems are possible, and they imply placing all electrodes at a 10% distance, or even less, at a 5%. The 10-10 electrode system, in Figure 9, fills intermediate sites halfway between those of the existing 10–20 system: according to the new nomenclature, electrodes labelled with odd numbers (1, 3, 5, 7, 9) on the left hemisphere are placed at increasing percentages of the inion-to-nasion distance: 1 at 10%, 3 at 20%, 5 at 30%, 7 at 40%, and 9 at 50% from the midline; the same applies symmetrically to the right hemisphere with even numbers. Extra letter codes to name intermediate electrode sites: AF, between Fp and F; FC, between F and C; FT, between F and T; CP, between C and P; TP, between T and P; PO, between P and O. Four electrodes of the 10–20 system can be renamed: T3 becomes T7; T4 becomes T8; T5 becomes P7; T6 becomes P8. It was thought that the labels T3/T4 and T5/T6 were inconsistent with respect to the other labels in the same sagittal line [10]. By using additional electrodes, high-density EEG provides a better spatial resolution: indeed, the higher the electrode density, the higher the spatial resolution.

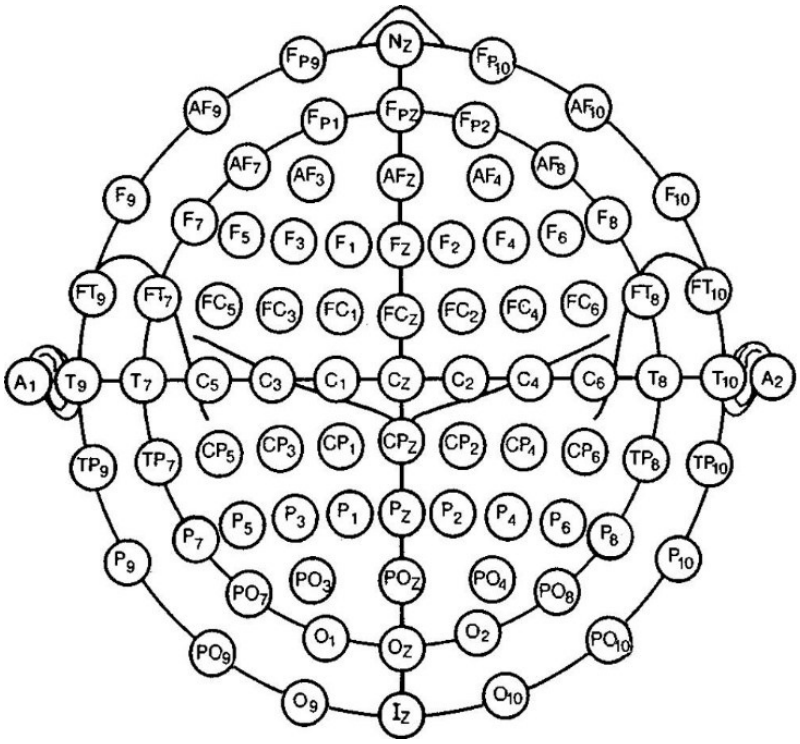

Figure 9. Electrodes positions in the 10-10 system [10].

EEG is recorded using the technology of the differential amplifier. The differential amplifier takes two electrical inputs and gives in output the difference between the two inputs. This is very useful to record and display very small electrical signals. EEG is not something that is absolute but the difference between two inputs, thus a relative measure and so any tracing in the EEG is a relative tracing [9]. The electrical signals (or electric potentials) recorded by the electrodes are transmitted to the amplifier. The amplifier has a dedicated channel for each active electrode placed on the scalp. Each EEG channel measures the voltage, specifically the potential difference between an active electrode and a reference electrode, known as the common recording reference. The common reference can either be the average voltage across all electrodes or from electrically silent areas, such as the ear's auricle. This configuration, in which each channel records the potential difference between a single scalp electrode and a common reference point, is known as a referential montage, in contrast, a bipolar montage would compare the voltage between adjacent pairs of electrodes without a common reference. The amplifier receives input from both the active and reference electrodes, with both referenced to a shared signal ground. The signals captured by the scalp electrodes have very low amplitudes, typically in the microvolt (μV) range. The electric potential at each electrode is influenced by non-brain signals, which can be transmitted to the scalp from other parts of the body. Since these nonbrain signals, which may even be large, are present at all scalp electrodes, they are effectively cancelled out when the potential at the reference electrode is subtracted from that of the active electrode. This process enhances the signal of interest. Each reference electrode corresponds to a

specific channel or derivation, and the resulting trace is the voltage difference between the active electrode and the reference. From the individual signals detected by the electrodes, a dataset representing the entire scalp is generated. All the electrodes are connected in what are called montages: logical, orderly arrangements of EEG derivations, or channels, created to display brain activity [9]. Montages can use computed values as reference, or they can use scalp electrodes as reference, and they can be classified in bipolar montages and referential montages. In a bipolar montage the electric potential of each electrode is linked and compared to an adjacent one. Each couple of electrodes define a channel or derivation. The tracing is obtained as the difference of voltage between the second and the first electrodes that define the derivation. String of tracing are determined in the bipolar montage, called chains. An example of a bipolar montage is the Double Banana Bipolar Montage is showed in the panel A of Figure 10, in this case each electrode is linked and compared to the one behind it and it is possible to identify the right temporal chain (Fp2-F8; F8-T8; T8-P8; P8-O2), the left temporal chain (Fp1-F7; F7-T7; T7-P7; P7-O1), the right parasagittal chain (Fp2-F4; F4-C4; C4- P4; P4-O2), the left parasagittal chain (Fp1-F3; F3-C3; C3-P3; P3-O1) and the central chain (Fz-Cz; Cz-Pz) [9]. Another example of a bipolar montage is the Circumferential Bipolar Montage, showed in panel B in Figure 10, which consists of linked bipolar derivations encircling the head, each electrode is linked and compared to the one adjacent forming a circumference around the head [9]. In this case all electrodes have a reference, but the middle and parasagittal regions are not explored. Instead in the Transverse Bipolar Montage, which is showed in panel C of Figure 10, each electrode is linked and compared to the one at the right or at the left. Chains are not in the sagittal direction, but in the transverse direction. Bipolar montages require the electrophysiological knowledge in order to have a correct interpretation of tracings [9].

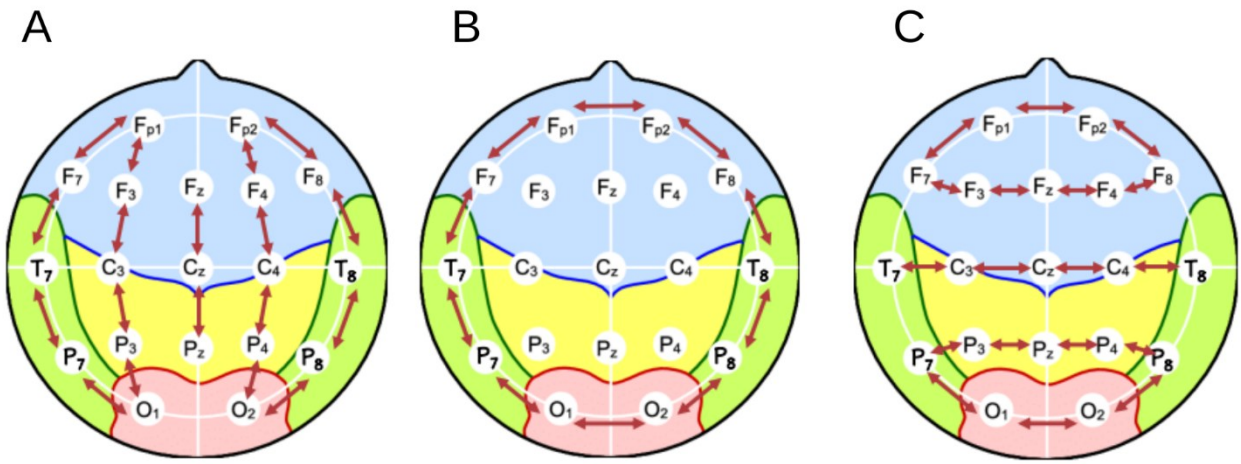

Figure 10. Examples of bipolar montages. (A) Double Banana Bipolar Montage (temporal, parasagittal, and central chains). (B) Circumferential Bipolar Montage. (C) Transverse Bipolar Montage [9].

In referential montages, instead, the electric potential of each electrode is linked and compared to a single common reference. Each referenced electrode defines a channel or derivation, i.e. a tracing. The tracing is obtained as the difference of voltage between the active electrode and the reference. The common reference can be the average of the voltage of all electrodes (average montage), or an electrode placed in an electrically silent area, as the auricle of the ear [9].

Standard EEG may be indicated to diagnose encephalopathy, to monitor coma etc, however, the standard 10-20 system does not include electrodes in some strategic areas for the diagnosis or monitoring of some diseases, as the inferior chain, at the level of the preauricular point. As a consequence, the activity originating or propagating from some regions cannot be acquired and this represent a limit if some pathologies manifest through them. A large array of electrodes is reserved for specific applications, such as electric source imaging for presurgical evaluation. Indeed, supplementary electrodes implies additional time and effort to be placed but provide a better coverage of the brain [10]. A compromise between the everyday routine and reliable detection represents a good solution if possible. Mathematical models are used for signal source localization, which consists in estimating the position of the neural generators responsible for the potentials measured on the scalp. This is achieved by combining mathematical algorithms with head models that describe the geometry and electrical properties of the brain, skull, and scalp tissues. A higher electrode density helps for a more precise localization. Thanks to engineering advances in EEG amplifiers, a much higher number of electrodes can be simultaneously recorded, and currently available systems allow EEG recording of 256 electrodes, or even more. Electrodes can be applied individually on the scalp or using expandable nets or caps. Large electrode arrays cover more brain regions, allowing a better

localization and definition of brain activity sources. The EEG recording is often acquired together with other electrophysiological signals, this technique is called polygraphy. It allows to obtain complementary and additional information, and to distinguish physiological artifacts in scalp EEG signals. The signals mostly acquired in polygraphy together with EEG are the electrocardiography, the electromyography and the electrooculography.

The EEG recording can be performed in different modalities, namely: routine EEG, ambulatory EEG, ambulatory video EEG and inpatient video EEG. Routine EEG monitoring is the recording of the brain's electrical activity for 20-40 minutes. The goal is to record the brain waves and determine if they show any abnormalities. Routine EEG is useful, but it can provide only limited information due to their short duration. Ambulatory EEG monitoring consists of a prolonged EEG recording performed at the patient's home. The acquisition is longer than the routine EEG lasting up to 24, 48 or 72 hours. In the case of ambulatory video EEG monitoring, modern EEG systems are equipped with cameras allowing simultaneous video recordings. Video recording is recommended because careful video-analysis of EEG events of which the origin could be doubtful can help to distinguish between cerebral cause or extracerebral cause. The association between the semiology and the EEG can provide useful information for the characterization of the episodes recorded through the EEG. Inpatient video EEG monitoring is similar to the ambulatory EEG monitoring, but it is performed in the hospital. Differently from the ambulatory video EEG, the signal is monitored on a regular basis by the physician, as the patient is under continuous medical supervision in the hospital. This setting also allows for the safe withdrawal of medications when needed, which would not be possible at home. For these reasons, inpatient video EEG is typically performed over three to five days, or even longer.

To recap, the EEG is a non-invasive technique that is able to directly detect the neuronal activity with a very high temporal resolution, in the order of milliseconds. Also, the equipment of EEG can be transportable and on the contrary of other techniques, the hardware costs lower and the EEG equipment does not aggravate claustrophobia. On the other hand, EEG is able to detect only the most superficial neuronal activity, it has a low spatial resolution and requires intense interpretation to hypothesize what brain areas are activated. Even though the preparation time differs based on the specific EEG device used, often the connection of electrodes to the scalp takes a long time, as it requires precise placement of many electrodes, and the use of gels, saline solutions or pastes. Moreover, the signal-to-noise ratio is low, meaning that sophisticated data analysis and a large number of recordings (or trials) per subject are needed to extract useful information from EEG. An artifact is any undesired signal, potential difference, perceived and acquired by the electrodes

originating by, in this case, an extracerebral source. It could be due to extra physiological factors, such as instrumental distortion or malfunction, or ambient electrical noise. The identification and elimination of artifacts is fundamental. The artifacts could be of technical origin: electrical noise from engines, bad electrode contact, electrode detachment, or power supply, 60 Hz in North America and 50 Hz in Europe. They can be also of biological origin, electrical signals generated within the human body by extracerebral physiological sources: cardiac electrical activity, eye movements, body and head movements, respiration or electrodermal. The eye blinks generate a slow signal corresponding to the movement of the eyelid, generating one of the most frequent artifacts encountered in routine EEG recordings, as they occur spontaneously several times per minute and produce a high-amplitude signal that can easily mask the underlying brain activity. The signal appears mainly in the prefrontal and frontal areas, and it is symmetrical between the two hemispheres. The eye movement generates slow signal as well, but in this case corresponds to the mechanical movement of the eyes. The eyes can be modelled as a dipole, which moves closer to or away from some electrodes and generate signal. The signal appears mainly in the frontal and temporal areas. These signals are not symmetrical between the two hemispheres and are propagated more often than blinks. Artifacts produced by frontal muscles generate high frequency signals, often much higher than neuronal signals. The main head muscle is the jaw, which can produce a considerable signal in the temporal area. Frontal muscles can also appear, since they are located just below the electrodes. The electrode artifacts are signals related to wire or electrodes movements producing a low-frequency artifact on an electrode, often with high amplitude. It is also possible that a mechanical artifact will appear following a head movement, and in this case a signal appears on several electrodes.

The EEG signal of interest for clinical and research applications typically lies within the frequency range of approximately 0.1 Hz to 70 Hz. This range encompasses the main EEG rhythms as well as slower and faster physiological activity of potential interest. Artifacts should be eliminated or at least attenuated. They could be within frequency ranges of EEG signal or outside frequency ranges of EEG signal. Several techniques have been developed for artifact elimination and most of them pertain specific kind of artifacts, while few of them aim at cancelling different kinds of artifacts. If the artifact is outside the frequency range of EEG signal it can be removed or reduced through digital filters, paying attention to the choice of the cut-off frequency, since the frequency components close to it are distorted. If the artifact is within the frequency range of EEG signal it is preferable to use alternative techniques with respect digital filters. Some approaches are aimed at separating the artifacts modelling the sources of extracerebral activity. There is also a class of algorithms, called blind source separation (BSS) algorithms, that do not rely on modelling the artifact to be removed, but on the isolation of components related to artifacts by the projection of data onto orthogonal or statistically

independent components [11]. It is a technique that estimates the individual source components from the knowledge of their mixtures at multiple sensors used for their acquisition. It is called blind because no other information is available than the mixed signals: the sources and the mixing modality, given by the mixing parameters, are unknown. According to the ratio between the number of source signals and the number of receiving sensors, the signal mixing model can be: overdetermined, if the number of sensors is higher than the number of sources; determined, if the number of sensors is equal to the number of sources; underdetermined, if the number of sensors is lower than the number of sources. According to the mixing modality, the signal mixing model can be divided into linear instantaneous mixing and convolutional mixing. The linear instantaneous mixing is the case when multiple speakers are talking concurrently in an anechoic room, thus without any reverberation effect or sound reflection. The convolutional mixing takes in consideration a more complex situation, where for example echo, reverberation and noise in general are present, then considering a more realistic situation [11]. Most of the signal mixing models deal with the instantaneous mixture of sources and only a few methods examine the situation of convolutive mixtures. It is worth noting that these few methods have been mainly developed for speech signals (e.g., in the context of the cocktail party problem), while convolutive mixing models for EEG signals remain relatively unexplored. In the case of the linear instantaneous mixing, the model can be represented in matrix form by eq. (1) or in equation form by eq. (2):

$$Y = A \cdot X \quad (1)$$

$$\forall i,\ y_i = \sum_j a_{ij} \cdot x_j \quad (2)$$

Where Y is the matrix containing the signals that are acquired by the sensors, A is the mixing matrix, which is the matrix containing the parameters that describe how the source signals linearly combine, and it has IxJ dimensions, instead, X is the matrix of the source signals. If we consider the possible presence of noise, always present in real acquisitions, the model can be described by eq. (3) and eq. (4):

$$Y = A \cdot X + N \quad (3)$$

$$\forall i,\ y_i = \sum_j a_{ij} \cdot x_j + n_{ij} \quad (4)$$

According to this model, each signal perceived by the sensor, hence the observation, is considered as the linear combination of the relative sources, plus a term representing the noises or perturbations. The only known terms are the observations. The estimation of the mixing matrix and sources is the aim of BSS. The situation brings to an ill-posed problem. In order to solve it, the typical approach is to make some assumptions about the sources and/or the mixing matrix. These assumptions are a priori

information that are not known, but simply supposed. A class of algorithms known as independent component analysis (ICA) can be effective at separating sources if there are multiple sensors located at different positions recording the signal produced by the sources. Since some sources are closer to a sensor than others, each sensor records a different weighted combination of the sources. Assuming to have as many sensors as the sources, additional assumptions about the statistical properties of sources often are sufficient to be able to derive the source signals from the mixtures recorded. The assumptions of the ICA are that the components are non-gaussian and statistically independent, as expressed by eq. (5):

$$P(x, y) = p(x)p(y) \quad (5)$$

where P(x,y) is the joint distribution of the variables x and y, p(x) is the probability distribution of x and p(y) is the probability distribution of y. From a mathematically standpoint, given some signals measured, the aim of ICA is to solve the mixing matrix so that the set of independent components or the set of sources are minimally independent [11]. The mixing matrix can be defined in two ways: as the matrix that minimizes the mutual information among all components, or as the matrix that maximizes the non-gaussianity. In the latter case the independent components can be found as the projections that maximize non-gaussianity.

1.2.2 Rhythms

A wave represents any change of the potential difference measured by the EEG recorder between pairs of electrodes, if it is originated within the brain, it is called brainwave, instead, if it is originated outside the brain, it is usually called extracerebral potential. The waveform refers to the shape or morphology of a wave. Each wave can be described by its waveform, which refers to the shape or morphology of a wave and its amplitude, which is defined as the height of the tracing relative to the baseline and is measured in microvolts (μV). In practice, the amplitude is often expressed as the peak-to-peak value, corresponding to the difference between the maximum and the minimum deviation from the baseline. If the EEG is rectified, more simply it is the height with respect the baseline. A normal brainwave of an adult individual can range from 10 to 100 μV, but it can reduce in case of response to a stimulus, as eye opening, in this case it is a transient attenuation, or as a result of pathological conditions. EEG waveforms are classified according to the frequency content. The most commonly studied waves, represented in Figure 11, are: delta (δ), with a frequency range from 0.5 to 4 Hz; theta (θ), from 4 to 7 Hz; alpha (α), from 8 to 12 Hz; beta (β), from 13 to 30Hz. Outside the conventional bandwidth, there could be detected infra slow oscillations/fluctuations (ISO/ISF), below 0.5Hz, and high-frequency oscillations (HFO), over 30Hz to 70 Hz, called gamma (γ). These non-conventional bandwidths could contain physiological and pathological relevant features of interest

for brain activity. Very high frequencies are not recorded in clinical practice because it requires sophisticated equipment and devices, since it involves high sampling frequencies, requiring wide space for storing, and low amplitudes, needing good electrodes and skin/electrode contacts [12].

Although most EEG studies do not examine signals below 1 Hz, the existence of such low-frequency activity has been known for many years. These signals, known as infra-slow oscillations (ISO), typically fall within the 0.01–0.1 Hz range. Notably, this frequency band has been found to be dominant in preterm neonates, suggesting a possible role in the development of neuronal connectivity during brain maturation. Interestingly, similar frequency components have also been observed in signals acquired with functional magnetic resonance imaging (fMRI), which relies on the blood oxygen level-dependent (BOLD) effect. Indeed, a link between EEG ISO and BOLD signals has been reported, and both appear to be modulated by changes in arousal levels, as measured by galvanic skin response (GSR), pupil size, and heart rate variability (HRV). Despite these findings, there is still no consensus regarding the temporal organization of EEG ISO: some studies report no clear peaks in this frequency band, while others describe prominent oscillations at approximately 0.1 Hz or 0.02 Hz. Furthermore, to date, no studies have explored the use of EEG ISO parameters as potential markers for distinguishing psychiatric patients from healthy controls, leaving this as an open issue for future research [13].

Delta wave (0.5–4 Hz) is recorded in deep sleep, it is significant in the frontocentral brain regions. The presence of delta waves when a person is awake may result in learning disabilities and attention deficit hyperactivity disorder (ADHD). Indeed, they may prevent mental concentration, restrict the ability to focus and maintain attention. Moreover, it is present in awake states in case of generalized encephalopathy and focal cerebral dysfunction. Intermittent rhythmic delta activity can manifest in different brain regions depending on age. Specifically, frontal intermittent rhythmic delta activity (FIRDA) is typically observed in adults, whereas occipital intermittent rhythmic delta activity (OIRDA) is more commonly seen in children. This age-dependent distribution suggests different underlying pathophysiological mechanisms, although both patterns are considered nonspecific EEG findings. Temporal intermittent rhythmic delta activity (TIRDA), on the other hand, is frequently seen in individuals with temporal lobe epilepsy and can affect one or both temporal lobes. Unlike FIRDA and OIRDA, TIRDA is considered an epileptiform abnormality, indicating a high risk for seizures originating from the affected temporal lobes [12].

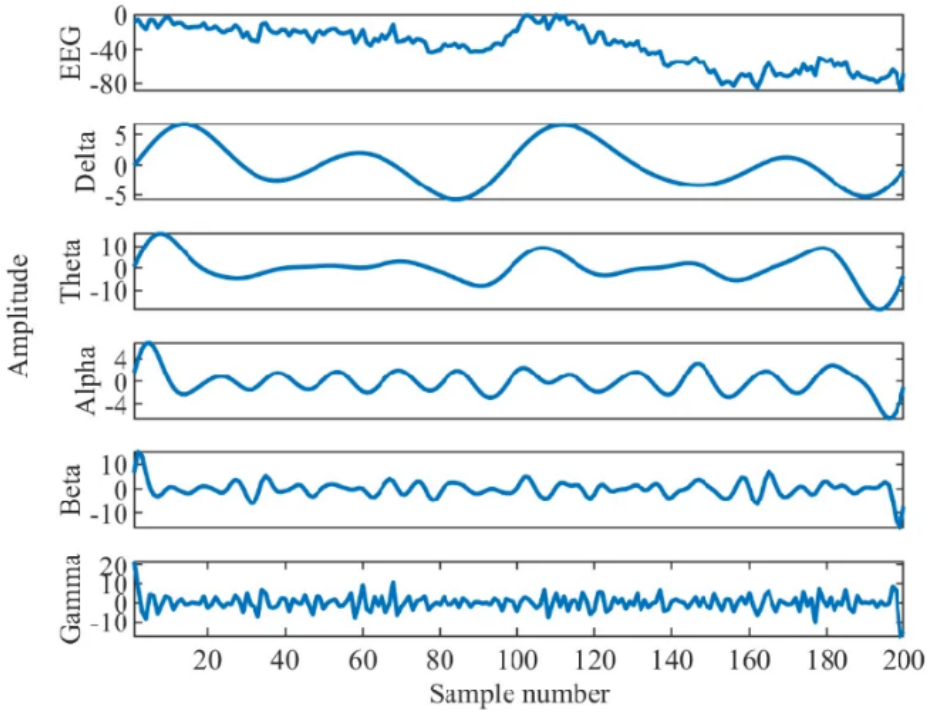

Figure 11. EEG rhythms [12].

Theta wave (4-8 Hz) is recorded in drowsiness and early stages of sleep. It reflects the state between wakefulness and sleep, it is associated with creativity, daydreaming, and imagination, it is significant in the frontocentral brain regions and then moves backward in place of alpha wave. The presence of theta waves when a person is awake may derive from cerebral dysfunction [12].

Alpha wave (8-12 Hz) is recorded in awake state, it is characteristic of the normal background activity of the adult EEG recording, it occurs whenever a person is alert, but not actively processing information. It is best seen with the eyes closed and during mental relaxation and is characteristically attenuated by eye-opening and mental effort, this phenomenon is called attenuation or blocking of alpha rhythm. Alpha amplitude is mostly below 50 μV in the adult, but often much higher in children. It is significant in the occipital brain region. It can be further divided into two sub-bands: 8-10 Hz and 10- 12 Hz. In diffuse encephalopathy, patients may show alpha activity which is nonreactive to internal or external stimuli [12].

Beta wave (12-35 Hz) is the most frequently recorded rhythm in normal adults and children. It reflects a state of consciousness at open eyes when the attention is focused on cognitive tasks, such as analytical problem solving, decision making, processing information, and on the perception of outside world, e.g. listening. It is significant in the frontal and central regions, while reduces going posteriorly.

Beta amplitude is mostly below 30 μV. Sometimes it is divided into three sub-bands: 12-15Hz, 15-18Hz, and 18- 30Hz. It may be absent or reduced in areas that suffer from cortical damages [12].

Some studies identify the sensorimotor rhythm (SMR) as an intermediate rhythm (12-15 Hz), in between the alpha and beta rhythms, thus shifting the beta rhythm to the 15-35 Hz range. The meaning of SMR is not fully understood and it is detectable in a person when the corresponding sensorimotor areas are idle. Therefore, the signal typically decreases in amplitude when the corresponding sensorimotor areas are activated. The SMR rhythm is hard to detect since it usually mixes with the alpha rhythm of the occipital region, which represents the most powerful and widespread rhythmic activity in the resting EEG, in fact this alpha activity often masks the SMR due to its higher amplitude and overlapping frequency range [14].

Gamma wave (35-70 Hz) is characterized by high frequencies, oscillating between 35 up to 70/100 Hz. It is associated with high levels of concentration and cognitive functioning. It has been attributed to sensory perception integrating different cortical areas. It is not associated with a particular region of the brain. These high frequencies have a limited clinical role with currently used technology, as they are particularly susceptible to muscle artifacts and environmental noise, and their low amplitude makes them difficult to distinguish from background activity without sophisticated signal processing. High frequencies require sophisticated EEG technology. Altered gamma activity can be observed in several cognitive and mood disorders, such as epilepsy, schizophrenia and Alzheimer's disease [15].

1.2.3. Engagement Indexes

As mentioned previously, the brain controls sensory processing, motor control, cognition, and attention, and, in general, every process that regulates our body. In particular, while performing continuous long-lasting or repetitive activities, subjects' brains are involved in functions that require sustained attention and, more generally, mental involvement [16]. Mental involvement can be defined as a brain state of focused vigilance, commitment, and active involvement, which is maintained over time while focusing on a task [16]. This state is characterized by a continuous level of alertness, rather than a response to a single stimulus, assessing mental involvement is relevant in several fields, including working environments, virtual reality, and medical applications. As a result, differences in the level of mental involvement between these two conditions may be reflected in EEG signals [16].

The fields of application of mental involvement assessment could be many others, ranging from the commercial field to evaluate the effectiveness of an advertising medium to the medical field for the evaluation of cognitive abilities and attention deficit disorders. One of the several ways to assess mental involvement is through the EEG, by computing engagement indexes from the spectral power

of EEG-derived brainwaves. According to the classification proposed by Wang et al. involvement indexes are indexes obtained from the spectral power of EEG-derived brainwaves and can be divided in basic and ratio indexes. The basic ones can be defined as the power or relative power of single brainwaves, while the ratio indexes can be defined as the ratio of powers and/or of power summations, thus including more than one single brainwave [16]. Indeed, although the literature agrees in attributing to the spectral power of each brainwave a close association with the cognitive patterns and mental state of subjects, this cannot always faithfully reflect variations of mental involvement, therefore an approach based on the ratio of spectral power of EEG-derived brainwaves seems to be preferable. The ratio indexes are also referred to as engagement indexes, terminology introduced by Pope et al. [16], remarking the fact that the relationship between brainwaves may reveal the level of mental involvement of the subject. Consequently, engagement indexes are ratios of functions involving the power spectral densities of more than one brainwave, as described by eq. (6):

$$SRI = \frac{f_1(a \cdot \delta, b \cdot \theta, c \cdot \alpha, d \cdot SMR, e \cdot \beta, g \cdot \gamma)}{f_2(h \cdot \delta, i \cdot \theta, j \cdot \alpha, k \cdot SMR, l \cdot \beta, m \cdot \gamma)} \quad (6)$$

where SRI stands for spectral ratio index, f_1 and f_1 are at least first-order functions in one of the power spectral densities, the coefficients a, b, c, d, e, g, h, l, m are binary numbers, then equal to either 1 or 0, and in any possible combination, except all equal to 1, since in that case SRI would be 1.

In this thesis 37 engagement indexes are considered, collected in the systematic review performed by Marcantoni et al. [16]. In addition to what has been mentioned previously, an index can be considered in its basic form, reported in Table 2, or in derived forms. Derived indexes are defined as indexes using the basic form of an original index but calculated over subsections of wave frequency bands using the introduction of weights into the terms of the formula, or using a formula where the terms are the original index (as in the case of indexes defined as reciprocals of the basic form) [16]. For the basic index I, the derived index can be computed as subtraction of the same index computed at the left and right brain hemispheres, reported by eq. (7), related to evaluation of the asymmetry of the index, which may be justified by lateralization of the brain:

$$I_{derived} = I_{left} - I_{right} \quad (7)$$

where the subscript refers to the position of electrodes on the two hemispheres. Another possible way to obtain a derived index is to compute the index I using a subsection of a wave, typically when dealing with δ, α, and β rhythms, or using the reciprocal of an index in its basic form. Furthermore, from I1 and its reciprocal form two involvement indexes, often defined as arousal index and valence index, are derived, specifically considering electrode positions F3, F4, AF3, AF4 of a standard

montage system including 81 electrodes, shown in Figure 8. Hence possible forms of the arousal and valence indexes can be obtained according to eq. (8), eq. (9), eq. (10) and eq. (11):

$$I_1\ (F3 + F4)\ (arousal)\ (8)$$

$$I_1\ (AF3 + AF4 + F3 + F4)\ (arousal)\ (9)$$

$$\frac{1}{I_1(AF3 + AF4 + F3 + F4)}\ (arousal)\ (10)$$

$$\frac{1}{I_1 F4} I_1(F3)\ (valence)\ (11)$$

Eq. (8), (9), (10) and (11) show that the same index is not always computed considering the same electrodes. Among the 37 indexes shown in Table 2, the most frequently used are I_1, I_2, I_3, and I_4, including their derived forms [16]. A standardization in the definition of these indexes is missing, both in the considered frequency bands and in the exploited electrodes and it is yet possible to define the best indexes for a specific application and context.

Table 2. The table collects the 37 engagement indexes in their basic form.

$I_1 = \frac{\beta}{\alpha}$	$I_9 = \frac{\theta + \alpha}{\alpha + \beta}$	$I_{16} = \frac{\delta + \theta}{\alpha + \beta}$	$I_{23} = \frac{\alpha + \beta}{\alpha + \theta}$	$I_{30} = \frac{\alpha + \beta}{\gamma}$
$I_2 = \frac{\beta}{\alpha + \theta}$	$I_{10} = \frac{\theta}{\alpha + \beta}$	$I_{17} = \frac{\delta}{\alpha}$	$I_{24} = \frac{\alpha}{\beta + \gamma}$	$I_{31} = \frac{\alpha + \gamma}{\theta + \delta}$
$I_3 = \frac{\beta}{\theta}$	$I_{11} = \frac{\theta + \alpha}{\gamma}$	$I_{18} = \frac{\delta}{\beta}$	$I_{25} = \frac{\delta + \theta + \alpha}{\beta + \gamma}$	$I_{32} = \frac{\theta + \alpha}{\delta}$
$I_4 = \frac{\theta}{\alpha}$	$I_{12} = \frac{\beta + \theta}{\alpha}$	$I_{19} = \frac{\theta}{\gamma}$	$I_{26} = \frac{\alpha}{\delta + \theta + \alpha}$	$I_{33} = \frac{\theta + \beta}{\alpha + \gamma}$
$I_5 = \frac{\theta}{\delta}$	$I_{13} = \frac{\delta + \theta}{\beta}$	$I_{20} = \frac{\alpha}{\gamma}$	$I_{27} = \frac{\alpha}{\theta + \alpha + \beta}$	$I_{34} = \frac{\beta + \gamma}{\delta + \theta}$
$I_6 = \frac{SMR}{\theta}$	$I_{14} = \frac{\delta + \theta + \alpha}{\beta}$	$I_{21} = \frac{SMR + \beta}{\theta}$	$I_{28} = \frac{\beta}{\theta + \gamma}$	$I_{35} = \frac{\delta + \alpha}{\theta + \gamma}$
$I_7 = \frac{SMR}{\beta}$	$I_{15} = \frac{\delta + \theta}{\alpha}$	$I_{22} = \frac{\theta + \alpha}{\beta + \gamma}$	$I_{29} = \frac{\beta + \gamma}{\delta}$	$I_{36} = \frac{\theta + \alpha}{\delta + \beta + \gamma}$
$I_8 = \frac{\alpha + \beta}{\delta}$				$I_{37} = \frac{\alpha + \beta}{\delta + \theta + \gamma}$

Beyond these engagement indexes, additional electrophysiological features have been extensively employed to characterize motor-related brain activity and to discriminate between ME and MI, these include event-related desynchronization (ERD), frontal alpha asymmetry, and functional connectivity measures such as coherence and phase-locking value (PLV). Event-Related Desynchronization (ERD) for the Alpha and Beta bands represents a decrease in oscillatory power over sensorimotor areas during motor preparation and execution, reflecting cortical activation. ERD is typically quantified on a logarithmic scale using the eq. (12):

$$ERD = 10 \cdot log10 \frac{(Ptask)}{(Pbaseline)} \quad (12)$$

where $P_{baseline}$ is the band power during the task and P_{task} is the band power during a reference baseline condition. This formulation yields negative values for desynchronization and positive values for synchronization and is typically computed for each channel and each trial.

Frontal Alpha Asymmetry quantifies the relative difference in Alpha power between the left and right frontal regions: it is computed as the difference between Alpha power at electrode F4 (right frontal region) and electrode F3 (left frontal region), divided by their sum as reported in the eq. (13):

$$\text{Frontal Alpha Asymmetry} = \frac{\alpha_{F4} - \alpha_{F3}}{\alpha_{F4} + \alpha_{F3}} \quad (13)$$

where α_{F4} and α_{F3} are the Alpha band powers at the right and left frontal electrodes, respectively. This metric ranges from −1 to +1: a positive value indicates greater Alpha power over the left hemisphere relative to the right, which is generally interpreted as greater right-hemisphere cortical activation; a negative value indicates greater Alpha power over the right hemisphere, reflecting greater left-hemisphere activation. Frontal Alpha Asymmetry has been associated with emotional, motivational, and cognitive control processes, as well as with attention and task engagement.

In addition, functional connectivity between homologous regions of the two hemispheres can be assessed through coherence and PLV. Coherence quantifies the linear correlation between two signals as a function of frequency, ranging from 0 to 1, where values close to 1 indicate a strong linear relationship. However, standard coherence is sensitive to volume conduction artifacts. To address this limitation, imaginary coherence isolates the imaginary component of the complex coherence, providing a more reliable estimate of true physiological connectivity. In contrast, PLV is a time-domain measure that captures phase consistency between two signals independently of their amplitude, as defined in eq. (14):

$$PLV = \left| \frac{1}{N} \sum_{t=1}^{N} e^{i(\varphi_1(t) - \varphi_2(t))} \right| \quad (14)$$

where $\varphi_1(t)$ and $\varphi_2(t)$ are the instantaneous phases of the two signals at time t, and N is the number of samples in the window. PLV ranges from 0 (random phase relationship) to 1 (perfect phase synchronization) and unlike coherence, PLV is particularly useful for detecting transient phase synchronizations that may reflect communication between distant cortical areas, such as those involved in motor preparation and execution, and it is less affected by amplitude fluctuations.

1.3 MOTOR EXECUTION VS MOTOR IMAGERY

Within the broader framework of brain electrophysiology, motor-related processes represent one of the most extensively studied domains. The generation and control of voluntary movement involve well-defined neural mechanisms that can be effectively observed through electroencephalographic recordings, particularly at the level of the sensorimotor cortex [17]. However, brain activity associated with movement is not limited to overt action. The nervous system is capable of activating motor representations even in the absence of actual movement, reflecting the existence of internal processes that mirror, anticipate, or simulate physical actions [18]. This duality between action and simulation provides a valuable perspective for investigating how the brain encodes movement-related information. In this thesis, two conditions are relevant: motor execution (ME) and motor imagery (MI). Although both are rooted in the same functional domain, they differ in their relationship with physical output, offering complementary insights into the organization of the motor system.

Motor execution (ME) refers to the actual performance of a voluntary movement. It encompasses the entire sensorimotor loop, including motor planning, activation of cortical and subcortical structures, transmission of neural signals to the muscles, and continuous integration of sensory feedback [19]. Motor imagery can be described as the internal rehearsal of a movement without any overt execution. During this process, individuals mentally simulate an action while remaining physically still [18]. Despite the absence of movement, motor imagery is not a purely abstract or symbolic activity; rather, it engages neural mechanisms that are closely related to those involved in actual execution [19]. At the behavioral level, numerous studies have suggested that both ME and MI are effective in motor skill learning and motor abilities rehabilitation. Moreover, evidence supports that ME and MI involve in similar cognitive processes, indicating that ME and MI share overlapping activated pattern in some critical regions including the supplementary motor area (SMA), premotor area (PMA), primary sensorimotor area (M1/S1), posterior parietal lobe (PPL), striatum, cerebellum and thalamus, in spite of their different volume and intensity of activation [20].

These aspects have gained increasing relevance not only for understanding motor control, but also for its applications in neurorehabilitation and neural engineering. From an electrophysiological perspective, motor execution is characterized by a cascade of measurable EEG phenomena. Among these, the most prominent is the event-related desynchronization (ERD) of the alpha (8–13 Hz) and beta (14–30 Hz) rhythms over the sensorimotor cortex, which reflects cortical activation [18,21,22]. ERD consists of a decrease in oscillatory power in a specific frequency band, which reflects the activation of underlying cortical areas; at the neuronal level, ERD is thought to result from a desynchronization of the firing patterns of large populations of neurons, which become more active

and less synchronized during task performance [23*]. In other words, when a cortical area is engaged in processing sensory information or preparing or executing a movement, the ongoing rhythmic activity in that region is attenuated, resulting in a power decrease in the EEG signal. Conversely, an increase in oscillatory power, known as event-related synchronization (ERS), is observed when cortical areas are in an idle or inhibited state [23*].This desynchronization is typically strong, sustained, and localized over contralateral central electrodes (e.g., C3/C4), in accordance with the somatotopic organization of the motor cortex. Motor imagery also induces ERD in similar frequency bands and cortical regions, confirming the involvement of motor-related neural circuits. However, compared to motor execution, MI is generally associated with weaker and shorter-lasting desynchronization, reflecting the absence of overt motor output and sensory feedback. In addition to oscillatory activity, lateralized readiness potentials (LRPs) recorded from central electrodes provide a marker of motor preparation and response selection, with differences in amplitude between execution and imagery conditions [24].

Beyond single-channel spectral power, EEG analysis can also capture functional interactions between different brain regions. Two widely used measures for this purpose are coherence and the phase-locking value (PLV). Coherence is a frequency-domain measure that quantifies the linear correlation between two signals at a given frequency, indicating the degree of synchrony in their amplitude and phase over time. It ranges from 0 to 1, where values close to 1 indicate a strong linear relationship [25]. However, standard coherence is sensitive to volume conduction artifacts, i.e., the passive spread of electrical activity from one source to nearby electrodes, which can produce spurious connectivity estimates. To address this limitation, imaginary coherence has been introduced: it isolates the imaginary component of the complex coherence, which is less affected by zero-lag coupling and therefore provides a more reliable estimate of true physiological connectivity [26]. In contrast to coherence, PLV is a time-domain measure that captures phase consistency between two signals independently of their amplitude [27]. It is computed from the instantaneous phases of the two signals, and ranges from 0 (random phase relationship) to 1 (perfect phase synchronization). PLV is particularly useful for detecting transient phase synchronizations that may reflect communication between distant cortical areas, such as those involved in motor preparation and execution [28].

Another important metric is frontal alpha asymmetry, which quantifies the relative difference in alpha power between the left and right frontal regions. Alpha activity is inversely related to cortical activation, meaning that lower alpha power reflects higher cortical activation. Thus, frontal alpha asymmetry provides an index of asymmetrical cortical activation between the two hemispheres, which has been associated with emotional and motivational processes, as well as with cognitive

control and attention [29]. It is computed as the difference between alpha power at right (F4) and left (F3) frontal electrodes, divided by their sum, yielding values ranging from -1 to +1. A positive value indicates greater alpha power over the left hemisphere relative to the right, which corresponds to greater right hemisphere cortical activation, and vice versa [30].

Neuroimaging studies (fMRI, fNIRS) and electrophysiological recordings (EEG, MEG) have consistently shown that MI elicits a weaker and shorter-lived ERD compared to ME, while preserving the somatotopic organization (e.g., hand versus foot laterality) and the temporal sequence of motor preparation. Spatially, EEG patterns during motor tasks reveal a clear organization of activity across the scalp. Motor execution typically produces focal and lateralized activation over sensorimotor regions, while motor imagery often involves a broader distribution, including premotor and parietal areas. This spatial information, combined with spectral and temporal features, forms the basis for the analysis and classification of motor-related EEG signals [31]. Motor imagery, in particular, plays a central role in BCI applications, because it does not require physical movement, MI can be used by individuals with severe motor impairments, such as those affected by stroke or spinal cord injury. By imagining specific movements, users can modulate their EEG signals, and thereby control external devices, such as robotic limbs or computer interfaces. Motor execution, although less commonly used as a control strategy in BCIs due to the requirement of physical movement, remains important as a reference condition. It provides a benchmark for understanding the neural mechanisms underlying motor-related signals and can be used in hybrid or training paradigms. Despite their potential, MI-based BCIs face several challenges, including variability in user performance, differences in neural patterns across subjects, and the relatively low signal-to-noise ratio of EEG recordings. These factors highlight the importance of identifying robust and discriminative features, as well as developing advanced signal processing and machine learning techniques. For this reason, the analysis of similarities and differences between ME and MI becomes particularly relevant, as it can inform the design of more effective decoding strategies and improve the reliability of BCI systems.

MOTIVATION AND RATIONALE OF THE THESIS

The study of motor execution and motor imagery has profound clinical and technological implications. Every year, millions of people worldwide lose the ability to move effectively due to neurological injury or disease. According to the World Health Organization (WHO), stroke remains the second leading cause of death globally, with over 12 million new cases annually [32]. Among stroke survivors, approximately 50–70% experience chronic upper limb hemiparesis, severely impacting quality of life [33]. Similarly, traumatic spinal cord injury (SCI) has an estimated global annual incidence of 250,000–500,000 cases, with many individuals developing complete or incomplete tetraplegia [34]. Neurodegenerative disorders such as amyotrophic lateral sclerosis (ALS), progressively abolish voluntary movement while often sparing cognitive functions and the ability to imagine movement [35].

In this context, brain–computer interfaces (BCIs) that decode motor imagery have emerged as a promising assistive and rehabilitative technology. MI-based BCIs can provide a non-muscular communication channel for severely paralyzed patients, enabling control of cursors, robotic arms, or exoskeletons [17, 18, 36]. Moreover, MI training, when paired with sensory feedback, has been shown to promote neuroplasticity and facilitate motor recovery in post-stroke rehabilitation (action observation and motor imagery therapy) [36]. However, the practical deployment of MI-BCIs is hampered by a fundamental gap: the neural signatures of MI are weaker, noisier, and more variable across subjects than those of ME [17,18,37]. While ME can be reliably decoded from EEG in most individuals, MI decoding performance remains suboptimal, especially in cross-subject scenarios [37,38]. This performance gap directly reflects the incomplete understanding of how MI differs from ME in terms of spectral, spatial, and temporal dynamics, and which features are robust across subjects [17,18,39].

Furthermore, the existing literature, although rich, presents contradictions: some studies report clear M1 activation during MI, others do not [24,31]; the role of beta rhythm dynamics is still debated [18,22]; and most importantly, the majority of studies have focused on group-level ERD comparisons between conditions, with limited attention to single-trial characterization, functional connectivity, and the systematic identification of discriminative features that generalize across individuals [37,38].

The general aim of the present thesis is to analyze and characterize EEG signals in order to investigate the differences in brain electrical activity elicited by motor execution and motor imagery, with the goal of identifying discriminative features that can inform both basic science and BCI applications. To achieve this aim, two specific objectives are defined:

1. To consolidate the existing evidences through a systematic literature review, identifying current methodological trends, established findings, and, most importantly, the remaining gaps and open questions that warrant further investigation.
2. To analyze data from a publicly available EEG dataset (the PhysioNet EEG Motor Movement/Imagery Dataset) in order to perform a quantitative characterization of the differences between MI and ME. Specifically, the analysis consist of a systematic preprocessing pipeline followed by the extraction of a comprehensive set of features: 5 rhythms, 22 spectral ratio indexes, ERD in the Alpha and Beta bands, frontal alpha asymmetry; and connectivity measures such as coherence and phase-locking value on symmetric electrode pairs. These features were then used to train and evaluate four different types of classifiers for each of the four movement types separately, using data from all subjects (inter-subject approach). Feature importance was computed for each subject individually, and an ensemble selection approach was then applied to retain only those features that were selected for at least 50% of the subjects. Model performance was evaluated using both 10-fold cross-validation and LOSO cross-validation, in order to assess the separability between ME and MI for four different movement types. Finally, performance was evaluated in terms of accuracy, sensitivity, specificity, and F1-score.

The ultimate goal is to provide a systematic characterization of the EEG features that best discriminate between motor execution and motor imagery, thereby identifying robust biomarkers that may be exploited to improve MI-based BCI reliability.

2. SYSTEMATIC LITERATURE REVIEW: STATE OF THE ART

A systematic bibliographic research was performed to identify and evaluate the existing scientific literature for the analysis and characterization of electroencephalographic (EEG) signals in order to investigate similarities and differences in brain electrical activity during motor execution (ME) and motor imagery (MI). The primary goal was to establish a foundation of current knowledge and identify methodological trends. The literature search was conducted in two major electronic bibliographic repositories, PubMed and Scopus, in December 2025. The search was confined to publications in English, with a final publication stage and published between January 1, 2000, and December 1, 2025. The search query was designed to capture studies involving EEG, the core comparison between MI and ME, the context of Brain-Computer Interfaces (BCIs), and the key psychological constructs of interest (engagement, cognitive load, involvement). The same search query was used to systematically look for documents in the two electronic bibliographic repositories.

The PubMed query was:

((EEG[All Fields]) OR (Electroencephalogra*[All Fields])) AND ("motor imagery"[All Fields]) AND ("motor execution"[All Fields]) AND (("brain-computer interface"[All Fields]) OR (BCI[All Fields])) AND ((engagement[All Fields]) OR ("cognitive load"[All Fields]) OR (involvement[All Fields]))

The Scopus query was:

TITLE-ABS-KEY ((EEG OR Electroencephalogra*) AND "motor imagery" AND "motor execution") AND ALL (("brain-computer interface" OR BCI) AND (engagement OR "cognitive load" OR involvement))

The initial search across the two databases yielded a total of 37 results: 9 on Pubmed and 28 on Scopus.

2.1 LITERATURE SEARCH STRATEGY AND DESIGN

All studies retrieved through the search query in PubMed and Scopus were screened with the purpose of including studies that:

- involve healthy human adult subjects, where ‘healthy subjects’ denotes a population not affected by any type of pathology (like patients with post-stroke hemiplegia, amyotrophic lateral sclerosis (ALS), primary lateral sclerosis (PLS));
- present a direct comparison between ME and MI tasks;

- although additional neuroimaging techniques such as functional Near-Infrared Spectroscopy (fNIRS) or functional Magnetic Resonance Imaging (fMRI), were also considered, as they provided significant contributions to understanding the neural correlates of MI/ME comparison and supported a more comprehensive anatomical and physiological contextualization.

On the other hand, the studies that:

- were conducted on children or adolescent populations;
- that were not available for retrieval;
- were not primarily focused on a direct comparison between MI and ME, and this includes investigations focused on:
    - ocular or eye-movement activity
    - inhibitory control tasks
    - mental preparation
    - intermuscular coherence
    - the effects of cardiac cycle on MI
    - brain connectivity in specific athlete groups (e.g., table tennis players)

were not included in this bibliographic research.

So, a final set of 14 publications was selected for in-depth analysis after applying the inclusion/exclusion criteria through a title and abstract screening. In PubMed the initial query returned 9 results; the application of exclusion criteria removed 5 studies, leaving 4 articles for inclusion, while in Scopus the initial query returned 28 results and after applying the specific exclusion criteria, 10 documents remained, including 8 articles and 2 conference papers. Figure 12 shows in detail the screening phases that led to the final selection of eligible studies.

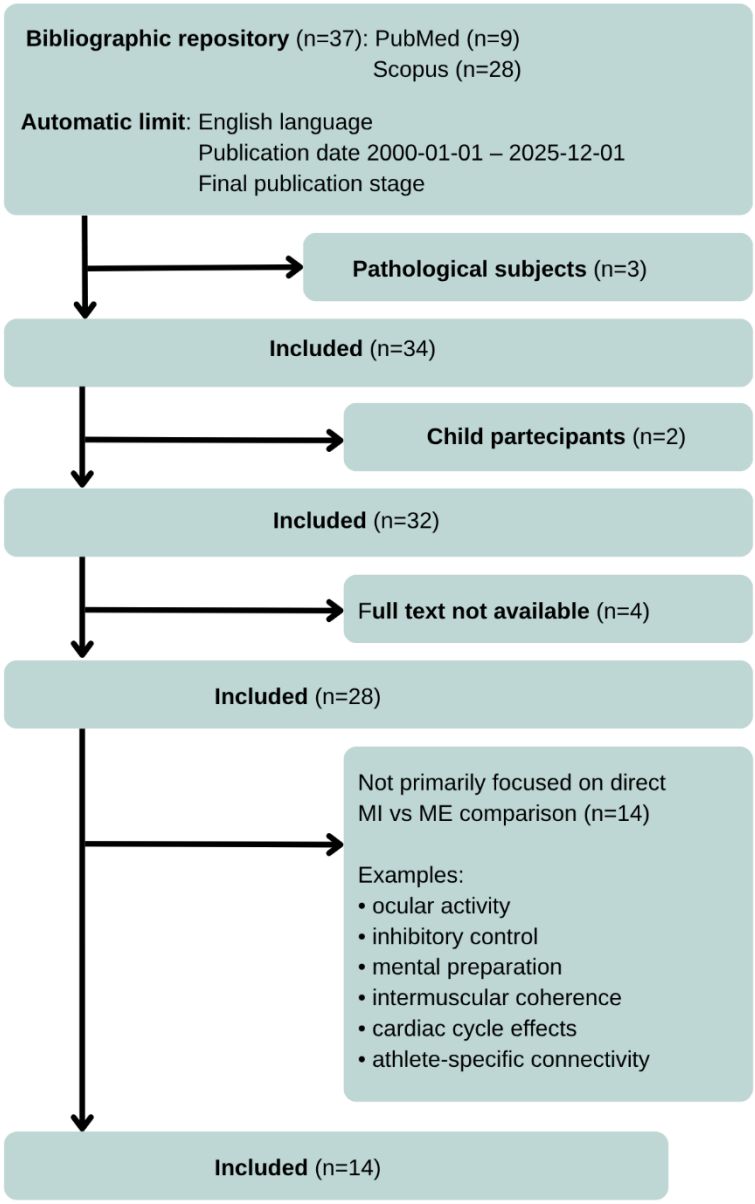

Figure 12. Flow diagram of the systematic review performed for the identification of eligible documents and enhancing of the screening criteria and selection.

2.2 DOCUMENTS INCLUDED

The results that the systematic research yield are reported into two complementary levels of analysis: physiological aspects such as neural substrates, activation patterns, movement types, population differences; and methodological/engineering aspects like acquisition techniques, signal features, experimental paradigms, analysis methods. Brain–Computer Interfaces (BCIs) establish a direct communication pathway between the human brain and the external world, operating as closed-loop systems that record brain activity, process the data to decode user intentions and deliver feedback

in the form of controlling an external device. Among the non-invasive methodologies for recording brain signals, EEG is widely used due to its high temporal resolution, affordability, and portability. EEG captures changes in the electrical fields generated by neural activity in the cerebral cortex through electrodes placed on the scalp, although it is limited by low spatial resolution and a low signal-to-noise ratio (SNR) [17]. Actual movement detection in BCIs is predicated on recognizing specific signal patterns associated with motor intents. For example, when a person imagines moving their right hand, specific patterns in the EEG signal correspond to the motor cortex area responsible for hand movement. These patterns, known as event-related desynchronization (ERD), can be used to trigger a command in a BCI system. Similarly, imagining movement, which is the mental simulation of movement without actual execution, results in detectable alterations in EEG signals. For individuals who have lost their ability to move due to diseases such as strokes or spinal cord injuries, this functionality is particularly valuable [18]. The bibliographic research provided a convergent view on the brain activity patterns associated with ME and MI. The findings can be synthesized into several key thematic areas.

Table 3. Methodological characteristics of the included studies: sample size and EEG acquisition device.

Study (Year)	Sample Size	Device Type
Duann & Chiou (2016)	13 healthy	EEG (64 channels)
Guo et al. (2024)	23 stroke, 21 healthy	EEG (64 channels)
Pérez-Velasco et al. (2025)	109 healthy	EEG (64 channels)
Bauer et al. (2015)	20 healthy	EEG (31 channels)
Amemiya et al. (2010)	33 healthy	NIRS
Fazli et al. (2011)	14 healthy	EEG (37 channels) + NIRS
Galdo-Alvarez et al. (2016)	18 healthy	EEG (28 channels)
Carrillo-de-la-Peña et al. (2006)	19 healthy	EEG (28 channels)
Nakayashiki et al. (2014)	11 healthy	EEG (8 channels)
Xu et al. (2019)	12 healthy	EEG (64 channels)
Zhi et al. (2025)	109 healthy	EEG (64 channels)
Fu et al. (2021)	10 healthy	fNIRS

Table 4. Study aims and classification approach of the included studies.

Study	Study Aim	Machine Learning for ME vs MI Classification
Duann & Chiou	Compare ERD during ME, MI, and MO to assess the reliability of MI/MO for BCI	No (Statistical analysis of ERD, not classification)
Guo et al.	Analyze brain connectivity (PMA/MA) during MI and ME in stroke patients	No (Correlation and PSD analysis, not classification)
Pérez-Velasco et al.	Evaluate transfer learning between ME and MI using deep learning without calibration for BCI	Yes (Deep Learning with EEGSym; 3-class (left/right/rest): 78.08% accuracy; 2-class (left/right): 86.21% accuracy)
Bauer et al.	Investigate the relationship between cortical networks (MI vs ME) and brain-robot interface control	No (Connectivity and network analysis, not classification)
Amemiya et al.	Evaluate intermanual transfer with MI vs ME training	No (Behavioral and NIRS measurement)
Fazli et al.	Assess whether NIRS can enhance SMR-EEG-based BCI during ME and MI	Yes (LDA for ME vs MI classification with EEG + NIRS; left/right hand classification: 78.2% with EEG-alone for MI, +5% improvement with hybrid approach)
Galdo-Alvarez et al.	Test functional equivalence between real and imagined performance in a stop-signal task	No (ERP analysis, not classification)
Carrillo-de-la-Peña et al.	Study functional equivalence of M-Ex/M-Im in a conflict task (hand vs foot)	No (LRP/N2/P3 analysis, not classification)
Nakayashiki et al.	Investigate how hand movement kinematics and kinetics modulate ERD	No (ERD analysis under different conditions, not classification)
Xu et al.	Improve single-trial mu-suppression (ERD) detection	No (Single-trial detection focus, not classification)
Zhi et al.	Develop a deep learning model for cross-subject MI/ME decoding without calibration (Domain Generalization)	Yes (Deep Learning with SCLDGN; left/right hand classification; average accuracy: 77.02%, LOSO validation)
Fu et al.	Classify fNIRS signals of real and imagined flexion/extension (arm) using Deep Belief Network	No (fNIRS modality)

All the studies agree regarding the substantial overlap in the neural circuits involved during ME and MI, supporting the theory of functional equivalence. Nevertheless, the more recent experiments using functional magnetic resonance imagery (fMRI) or magnetoencephalography (MEG) continue to produce conflicting results: while some studies find that the primary motor cortex (M1) is activated, although to a lesser degree, during MI, others fail to confirm the role of M1 either when subjects imagine themselves explicitly moving a limb or in implicit MI tasks that require mental rotation of the hand [24]. Importantly, the notion of functional equivalence must be nuanced: “equivalent” does not mean “equal”. ERP study using precueing tasks revealed that while both MI and ME elicit Lateralized Readiness Potentials (LRPs) with similar morphology and latency, the amplitude of later component (LRP-2), which reflects the late stage of motor preparation when all movement parameters are specified, is significantly larger during execution, reflecting stronger activation of M1 when full movement parameters are specified. This evidence refines the functional equivalence hypothesis by showing that MI engages M1, but with reduced intensity compared to ME [31]. In fact, both tasks consistently activate the core sensorimotor system. This includes the contralateral primary motor cortex (M1), premotor cortex (PMC), supplementary motor area (SMA), primary (S1) and secondary (S2) somatosensory cortices, the cerebellum, parietal lobes, and striatal structures like the putamen [19]. This convergence of activation patterns is visually summarized in Figure 13, which compares brain activity maps for ME and MI. The figure highlights the extensive overlap across cortical and subcortical regions, while also revealing differences in activation intensity and distribution. For instance, MI shows stronger involvement of the supplementary motor area and caudate nucleus, whereas ME elicits more robust activation in M1, S1, S2, and cerebellar regions [19]. Such evidence reinforces the notion that both processes rely on a shared motor representation system, yet differ in the degree of somatosensory and motor output engagement.

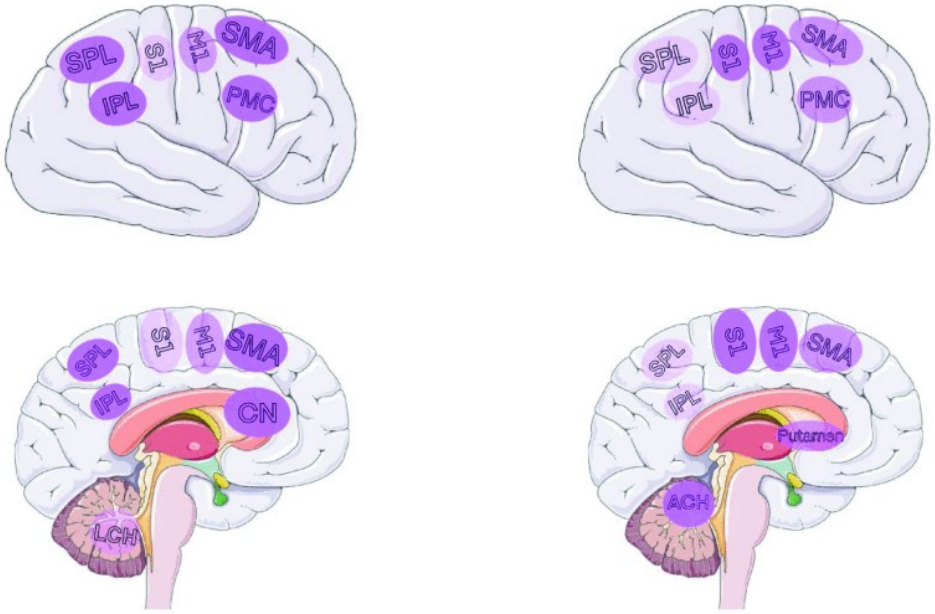

Figure 13. Brain activation maps during motor imagery (left) and motor execution (right). The intensity of color indicates the strength of activation in each region. Overlapping sites include PMC, M1, S1, S2, SMA, striatum, cerebellar hemispheres, and parietal lobes. Stronger activation in SMA and caudate nucleus is observed during MI, while ME elicits more robust activity in M1, S1, S2, and cerebellar regions [19].

The LRP is an event-related potential (ERP) component associated with motor preparation, generated in the primary motor cortex [24]. It is obtained by contrasting activity over contralateral and ipsilateral motor electrodes (typically C3 and C4), thereby isolating lateralized motor activity while removing non-motor contributions. A key feature of the LRP is its polarity inversion depending on the limb involved: hand movements elicit a negative deflection, whereas foot movements elicit a positive deflection, reflecting the somatotopic organization of M1 [24][19]. This phenomenon is clearly illustrated in Figure 14, where LRPs obtained during both ME and MI show opposite polarities for hand versus foot movements. Importantly, the inversion of polarity is preserved even when subjects only imagine the movement, providing compelling evidence that MI engages the same somatotopic representations in M1 as overt execution. Figure 14 also highlights that incongruent trials produce a premature preparation of the incorrect response, visible as a positive deflection in the LRP waveform, again observed in both execution and imagery conditions. In the Eriksen flanker task used in this study, each trial consists of a central target arrow flanked by two arrows on each side. In congruent trials, all arrows point in the same direction, facilitating response selection. In incongruent trials, the flanker arrows point in the opposite direction to the target, creating response conflict. This conflict induces two well-documented effects on the LRP. First, it prolongs LRP latency, reflecting delayed

response selection due to interference from the incompatible flankers, and second, it generates an initial positive deflection in the LRP waveform, which indexes the subthreshold activation of the incorrect response (the hand indicated by the flankers) before the correct response is ultimately selected and prepared. The fact that both effects are observed during motor imagery as well as during actual execution demonstrates that imagined movements are subject to the same conflict monitoring mechanisms and follow the same temporal dynamics as real movements. This provides strong evidence that motor imagery engages not only motor preparation areas but also higher-order cognitive control processes involved in resolving response conflict. Such findings, moreover, confirm that MI engages precise cortical representations for each limb and substantiate the functional equivalence hypothesis by demonstrating the involvement of the M1 in MI [24].

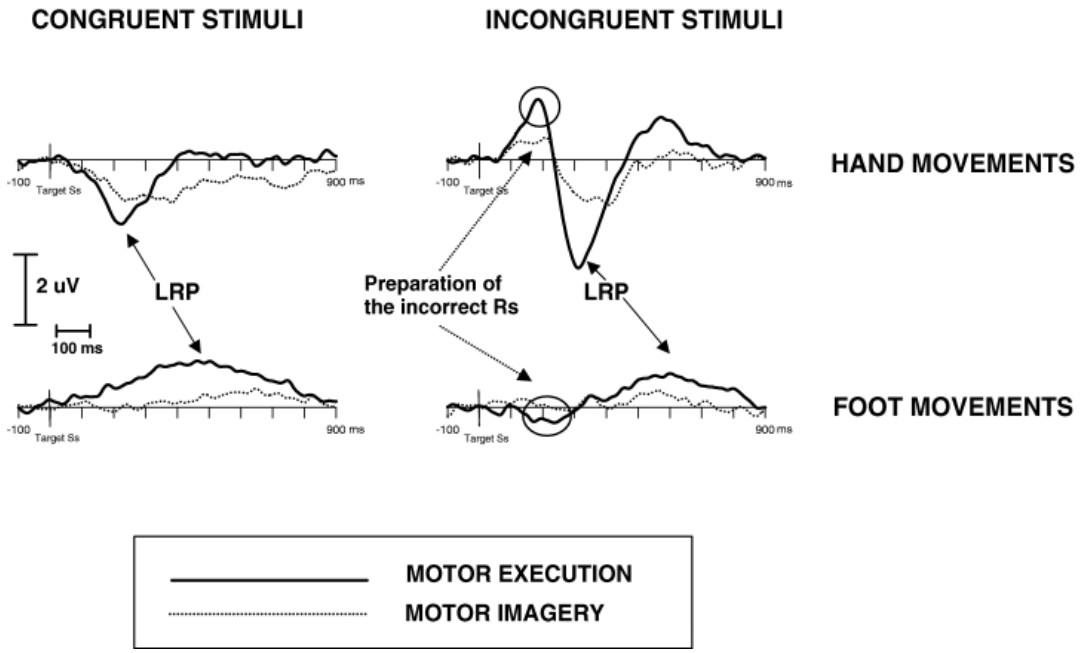

Figure 14. Lateralized Readiness Potentials (LRPs) obtained for hand (upper panels) and foot (lower panels) movements in congruent and incongruent trials, during both motor execution (ME) and motor imagery (MI). Note that the inversion of LRP polarity characterizes foot responses, and that this inversion is also present during motor imagery. The figure further shows premature preparation of incorrect responses in incongruent trials, visible as a positive deflection in the LRP waveform [24].

Duann and Chiou (2016) further demonstrated the consistency of motor-related EEG components across subjects by applying Independent Component Analysis (ICA) and clustering procedures to identify a right motor-related component in each participant. The experimental design included three different task: movement execution (actual hand clenching), movement imagery (kinesthetic imagination of the same action), and movement observation (watching a video of someone else

performing the action), with 20 trials for each condition presented in pseudorandomized order within the same experimental run. By applying ICA to the concatenated data from all three conditions, they isolated a common right motor-related component. Subsequently, they computed the event-related desynchronization (ERD) separately for each condition. The grand-average scalp topography of these components (Figure 15) highlights the common localization of the α rhythm suppression in the right motor cortex, despite inter-subject variability. These findings provide robust electrophysiological evidence that ERD responses are consistently observed during execution, imagery, and even observation tasks, reinforcing the functional overlap of motor-related brain areas [21].

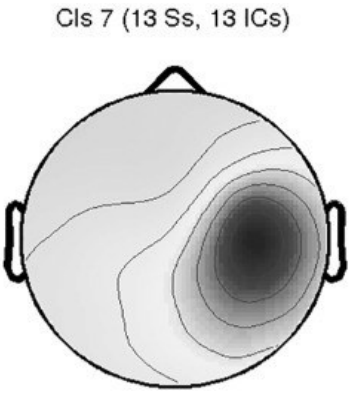

Figure 15. Grand-average scalp topography of the right motor-related independent EEG component derived from the mean of 13 participants [21].

Although the networks overlap, clear differences can be observed in the intensity, duration, and spatial distribution of neural activation. In fact, the Event-Related Desynchronization (ERD) in the α (8-13 Hz) and β (14-30 Hz) rhythms over the sensorimotor cortex is a primary EEG biomarker. As commonly reported in the literature, ERD is quantified on a logarithmic scale in decibels ($dB = 10 \times \log_{10}(Power\_task/Power\_baseline)$) to normalize inter-individual variability in baseline EEG amplitude and to render power decreases and increases symmetric. During ME, the ERD is significantly stronger (approx. -5 dB) and longer-lasting (>2000 ms). In contrast, MI generates a weaker ERD (around -2.5 to -3 dB) that is shorter, typically lasting 600–700 ms. This indicates a weaker and shorter electric signal produced during the MI. Complementary evidence comes from Nakayashiki et al. (2014), who systematically investigated how kinematic (movement speed) and kinetic (motor load) factors modulate ERD during repetitive hand grasping. They found that α and β ERD were significantly weakened under isometric “Hold” conditions, whereas variations in motor load did not produce significant differences. These results suggest that ERD strength reflects changes in hand posture and proprioceptive variation rather than the absolute motor command output [22].

Figure 16 illustrates the grand mean conditional α ERD time courses across all subjects for the two motor conditions considered in this thesis: ME (red) and MI (green) [21]. The error bars represent the standard error of the mean ERD response, while the dotted lines at the bottom indicate the time intervals of significant α suppression relative to baseline ($p < 0.05$). As shown, the ME condition elicited a stronger and more sustained ERD, lasting for more than 2000 ms, whereas the MI condition induced a weaker suppression with a shorter duration of approximately 600–700 ms. This comparison highlights the fundamental differences between ME and MI [21].

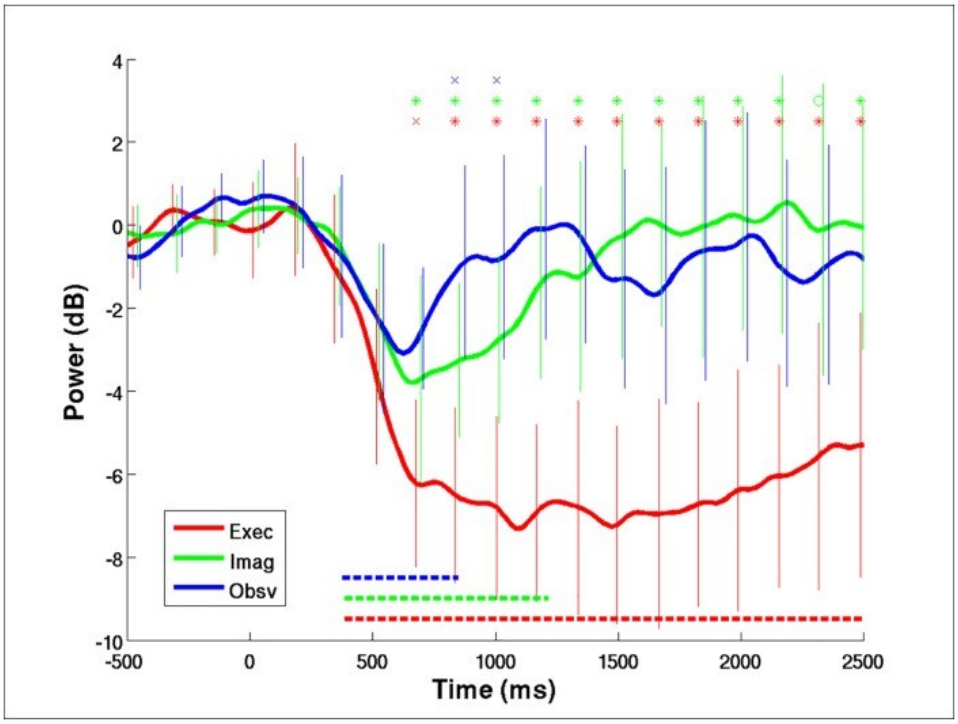

Figure 16. Grand mean conditional α ERD time courses (8–13 Hz) aligned to the onset of the execution cue across all subjects. Red line: movement execution (ME); green line: motor imagery (MI). Error bars indicate the standard error of the mean. Dotted lines at the bottom denote significant alpha suppression relative to baseline ($p < 0.05$) [21].

Additional differences can be observed in the spatial distribution of cortical activity. As illustrated in Figure 17, MI engages a broader set of cortical regions, including the supplementary motor area (SMA), premotor cortex (PMC), and parietal EEG sites, specifically CP3 and CP4, which correspond to electrodes positioned over the left and right parietal cortex in the international 10–20 system [39]. The figure also highlights the role of BCI familiarity in modulating cortical recruitment. Specifically, subjects with prior BCI experience (familiar users) exhibit a more focused and predominantly contralateral activation pattern, whereas novice users (BCI-naïve) display a broader, more bilateral recruitment of sensorimotor areas. This distinction suggests that learning and familiarity with the BCI paradigm can shape the neural substrates recruited during motor imagery, potentially reflecting more

efficient cortical processing with practice [39]. This reflects the higher cognitive demand, the internal monitoring, and the suppression of motor output required for mental simulation. Consistent with this, Amemiya et al. (2010) demonstrated that motor imagery training improved both ipsilateral and contralateral hand performance, whereas motor execution training enhanced only the trained limb. This effector-independent tendency of MI highlights its role in abstract sequence acquisition and contrasts with the effector-dependent nature of ME [40]. On the other hand, Figure 18 shows that ME elicits stronger and more lateralized activation in M1, S1/S2, and anterior cerebellar regions, correlating with the generation of efferent commands and the processing of real-time proprioceptive feedback. These topographical differences are consistent with the identification of optimal electrode subsets (Core Channel Selection) for classification of ME and MI, highlighting both the overlap around central electrodes (e.g., C3, C4, FC1, FC2) and the broader recruitment of associative regions during MI [32].

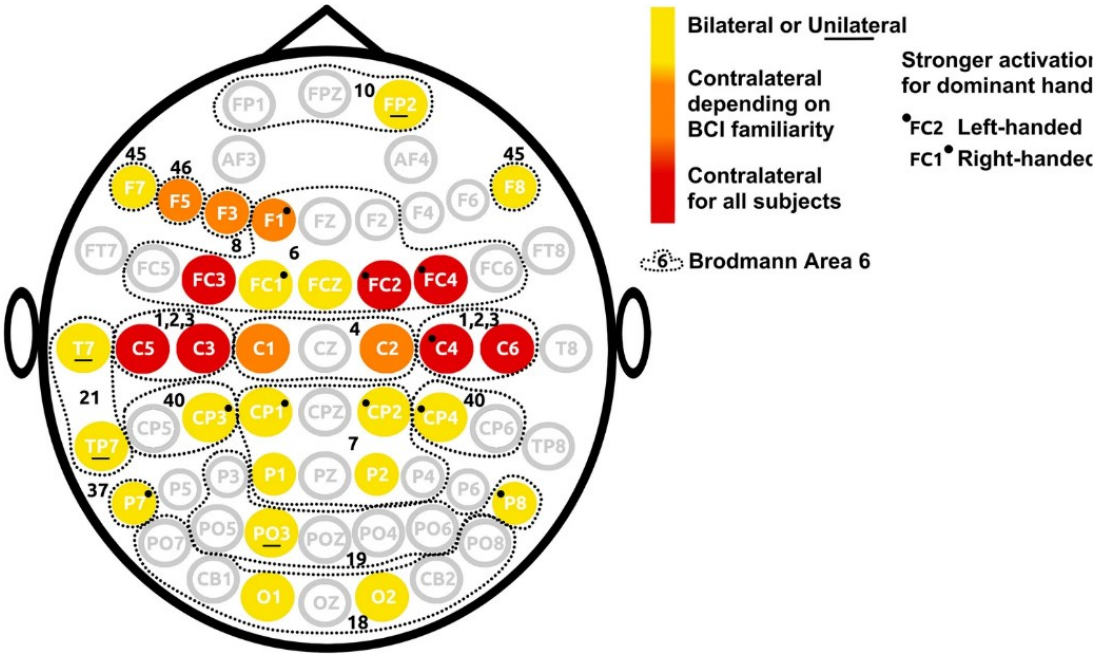

Figure 17. Motor imagery paradigm: activated electrodes with their corresponding Brodmann areas and handedness-linked laterality. The figure highlights the broader cortical recruitment during MI, including SMA, PMC, and parietal regions [39].

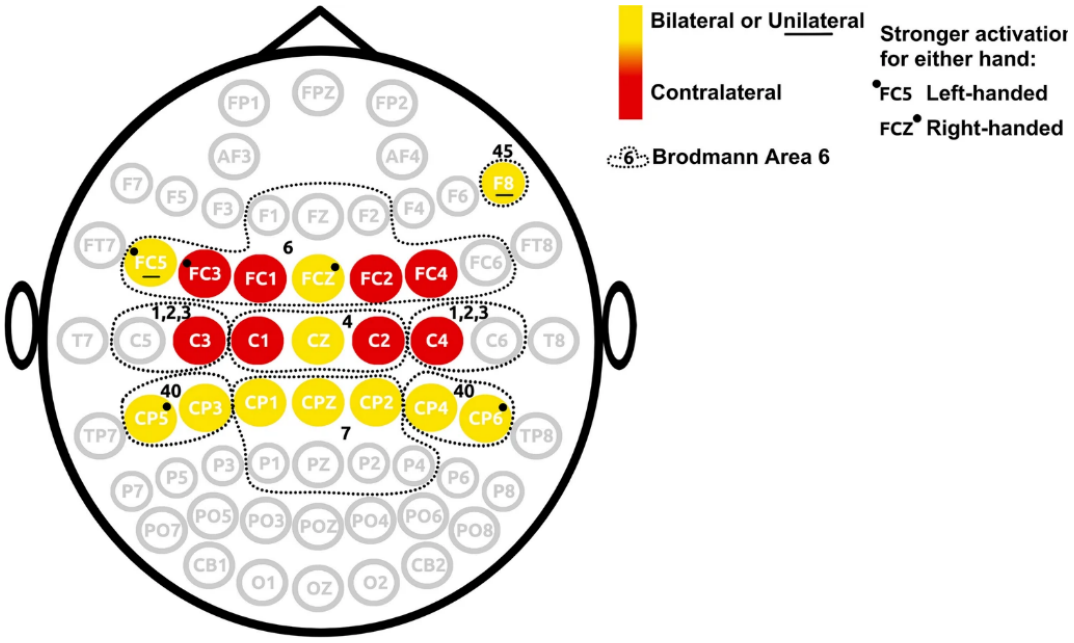

Figure 18. Motor execution paradigm: activated electrodes with their corresponding Brodmann areas and handedness-linked laterality. The figure illustrates the stronger and more lateralized activation in M1, S1/S2, and cerebellar regions during ME [39].

The key differences become evident when viewed through the perspective of motor control hierarchies, a theoretical framework that conceptualizes motor control as organized in a cascade of levels, from higher-order cognitive areas (such as prefrontal and premotor cortices) involved in planning and strategy, down to the primary motor cortex (M1) responsible for executing the final motor command, with continuous sensory feedback loops modulating the output at each level. From this hierarchical perspective, ME involves the full sequence of processes, from high-level planning to motor output, with continuous adjustments provided by sensory feedback. The pronounced and sustained ERD clearly reflects this comprehensive engagement, while MI is primarily a planning process with inhibited execution. It engages preparatory and planning stages, as shown by SMA and PMC activity, and even accesses motor command representations in M1. However, the final efferent pathway is blocked or suppressed, likely due to prefrontal involvement. LRP data provide strong evidence: while the early preparation component is identical in MI and ME, the later component associated with parameter specification and execution is significantly reduced in MI. This indicates that MI may not fully encode kinetic parameters such as force or fine sequence timing [40].

A major practical challenge highlighted across studies is the high degree of inter-subject variability. Developing an accurate decoding system for cross-subject applications remains challenging due to domain shift problem, which refers to the statistical distribution mismatch between training data (source domain) and test data (target domain). In the context of EEG-based motor decoding, this issue

arises from different sources of variability, such as differences in equipment, subjects, sessions, and even trials, which hinder the ability of a model trained on one subject to achieve acceptable performance when applied to another subject [37]. In other words, a classifier that works well for one person may fail for another because the EEG signal characteristics differ significantly across individuals. So, significant differences across individuals can be observed in the morphology of hemodynamic responses (in fNIRS), in ERD patterns, in the intensity of activation, and even in the mental strategies employed, so each subject's neural profile can be viewed as a unique "fingerprint." But this can lead to a 'domain shift' problem in machine learning: a model trained on one subject often performs poorly when applied to another. So, it is possible to identify distinct networks: the MI network is characterized by parietal-to-motor and motor-to-prefrontal inhibitory flows, whereas the ME network shows strong inter-hemispheric motor connectivity. It is important to underline that proficiency in MI does not imply proficiency in ME. These distinct network configurations also contribute to the inter-individual variability observed in neurophysiological responses. Specifically, Xu, Huang, and Duann (2025) demonstrated that the latency of μ-suppression (i.e., the timing of alpha power decrease) varies significantly across individuals, while remaining relatively stable within the same person. This suggests that each individual's unique neural "fingerprint" is not limited to the spatial distribution of activation or the intensity of ERD, but extends also to the temporal dynamics of motor-related oscillations. Consequently, a model or parameter setting that works for one subject (e.g., a fixed latency window for detecting mu-suppression) may fail for another, precisely because their underlying MI and ME networks are organized differently in terms of both connectivity patterns and timing. This reinforces the need for subject-specific approaches in BCI applications, as generalized settings are unlikely to accommodate the full range of inter-individual variability [38].

The α rhythm ERD represents the most reliable feature for distinguishing between MI and ME, with the first 0.5–1 second after the stimulus presentation as the most informative window for classification. For what concerns the fNIRS, the oxy-hemoglobin (HbO) signal within a 0–8 second interval provides strong discriminative power. Consistent with this, Fu et al. (2021) showed that deep belief networks (DBNs) trained on HbO features can classify flexion and extension imagery of both arms with an average accuracy of 78.19%. Their findings confirm the feasibility of combining fNIRS with deep learning approaches for MI recognition, while also stressing the importance of subject-specific models [41]. In parallel, hybrid BCI evidence shows that combining EEG with fNIRS improves motor imagery decoding: Fazli et al. (2012) reported significant accuracy gains (5% on average) in over 90% of subjects, indicating that the two modalities contribute complementary information despite the slower hemodynamic response [42].

The integration of hybrid approaches, such as brain–robot interfaces (BRI), may provide a practical pathway to overcome variability. As shown by Bauer et al. (2015), motor imagery and motor execution rely on partially distinct cortical networks: MI engages a network connecting left parietal and motor areas with the right prefrontal cortex, while ME is characterized by inter-hemispheric transmission from the left to the right motor areas. Importantly, these two networks are orthogonal, meaning that proficiency in one does not imply proficiency in the other. However, a BRI that provides haptic/proprioceptive feedback during motor imagery (i.e., passive movement of the patient's hand by a robot while the patient imagines the movement) can recruit both networks simultaneously. The passive movement activates the proprioceptive system and, consequently, the primary motor cortex, thereby engaging the motor execution network, while the instruction to imagine engages the motor imagery network. In this way, the BRI acts as a "backdoor" to the motor execution system, bridging the gap between the two networks and enhancing the feasibility of MI-based rehabilitation strategies, even in patients with severe motor impairments [36]. To address inter-subject variability, advanced machine learning approaches such as Domain Generalization (DG) have been developed. These methods aim to learn universal feature representations from multiple source subjects that can generalize to entirely new individuals without recalibration.

Table 5. Comparative overview of neural activation patterns during Motor Execution (ME) and Motor Imagery (MI). While both tasks share a substantial overlap in core sensorimotor circuits, quantitative differences in ERD amplitude and duration, as well as qualitative distinctions in LRP components and motor output, highlight the divergent functional profiles of ME and MI.

Aspect	Motor Execution (ME)	Motor Imagery (MI)
Cortical activation	M1, PMC, SMA, S1/S2, cerebellum, parietal, striatum	Same core areas + stronger SMA and fronto-parietal involvement
ERD amplitude	Strong (-5 dB)	Weaker (-2.5/ -3 dB)
ERD duration	>2000 ms post-cue	600–700 ms
Key electrodes	FC4, FC2, FC1, FC3, C2, C1, C4, C3	FC4, FC2, FC1, C4, C6, C5, C3, CP3, CP1
LRP	High-amplitude	Low-amplitude LRP
Motor output	Real execution with sensory feedback	Planning with inhibited output (prefrontal suppression)

2.3 OBSERVATIONS

Beyond the ERD strength comparison, the present study requires a comprehensive characterization that addresses spatial, spectral-temporal, and connectivity aspects. From a spatial perspective, ERD topographical maps during ME and MI must be systematically compared across the scalp, with particular attention to the shift from central to parietal involvement. Equally important is the analysis of spectral-temporal dynamics; rather than restricting the investigation to predefined frequency bands, the time–frequency evolution of the signals should be examined, as this captures transient dynamics and task-related modulations that might otherwise be overlooked. It is expected that MI will display a weaker ERD that diminishes earlier in both the α and β ranges, whereas ME is characterized by a more sustained suppression. Finally, functional connectivity may represent a crucial differentiating factor; ME is hypothesized to elicit stronger and more focused connectivity within the contralateral sensorimotor network, in contrast, MI may involve more diffuse or enhanced fronto-parietal connectivity, reflecting the engagement of cognitive control mechanisms. To capture these interactions, metrics such as coherence or phase-locking value are usually employed.

The literature highlights specific features that should guide the development of an analytical framework. The primary discriminants are represented by the amplitude and the duration of the α-rhythm ERD over the contralateral sensorimotor cortex (e.g., electrodes C3/C4). In contrast, the β rhythm dynamics and the spatial activation pattern (e.g., the involvement of electrodes CP3/CP4 in MI) represent secondary features that can enhance the discrimination between motor execution and motor imagery, especially in subjects for whom the alpha ERD alone does not provide a reliable separation between the two conditions. Analyses should focus on the 0-1000 ms post-stimulus interval, paying special attention to the 500–1000 ms window, during which differences in motor command specification are likely to be most evident. The study design must address variability as well; subjects should be considered based on the quality of the EEG signals. Their data should be analyzed to identify neurophysiological correlates of performance (baseline α power, strength of ERD, connectivity patterns). The analysis should then identify which extracted features remain more consistent across subjects for each task. In this context, domain adaptation enhances performance by calibrating the model with data from the target subject, whereas domain generalization seeks to learn subject-independent representations from multiple source subjects, ultimately aiming for zero-shot generalization as the ideal “ready-to-use” scenario.

3. MATERIALS AND METHOD

3.1 DATASET DESCRIPTION

The EEG Motor Movement/Imagery Dataset was employed to support my work: it is publicly available via PhysioNet and consists of over 1500 one- and two-minute electroencephalographic (EEG) recordings. The dataset comprises recordings from 109 healthy adult volunteers, recruited to participate in a controlled experimental protocol involving motor execution and motor imagery tasks. EEG signals were acquired using the BCI2000 platform, an open-source general-purpose system for brain-computer interface (BCI) research (http://www.bci2000.org) [43]. Each subject performed 14 experimental runs: one-minute baseline run with eyes open; one-minute baseline run with eyes closed and runs 3–14 are three two-minutes runs of each of four tasks (motor execution or motor imagery tasks). The tasks performed in runs 3-14 consists in:

1. When a target appears on either the left or the right side of the screen, the subject opens and closes the corresponding fist until the target disappears. Then the subject relaxes.
2. When a target appears on either the left or the right side of the screen the subject imagines opening and closing the corresponding fist until the target disappears. Then the subject relaxes.
3. When a target appears on either the top or the bottom of the screen the subject opens and closes either both fists (if the target is on top) or both feet (if the target is on the bottom) until the target disappears. Then the subject relaxes.
4. When a target appears on either the top or the bottom of the screen the subject imagines opening and closing either both fists (if the target is on top) or both feet (if the target is on the bottom) until the target disappears. Then the subject relaxes.

So the experimental runs are:

1. Baseline, eyes open
2. Baseline, eyes closed
3. Task 1 (open and close left or right fist)
4. Task 2 (imagine opening and closing left or right fist)
5. Task 3 (open and close both fists or both feet)
6. Task 4 (imagine opening and closing both fists or both feet)
7. Task 1
8. Task 2
9. Task 3

10. Task 4
11. Task 1
12. Task 2
13. Task 3
14. Task 4

As shown in Figure 19; the first two runs (R01 and R02) were one-minute baselines, with eyes open and eyes closed, respectively, runs R03 to R14 last two minute and contain a sequence of rest periods (T0) and task periods (T1 or T2), as illustrated in the Figure 19. T0 corresponds to rest. T1 corresponds to the onset of left-fist movement/imagery (in unilateral runs) or both-fists movement/imagery (in bilateral runs). T2 corresponds to the onset of right-fist movement/imagery (in unilateral runs) or both-feet movement/imagery (in bilateral runs).

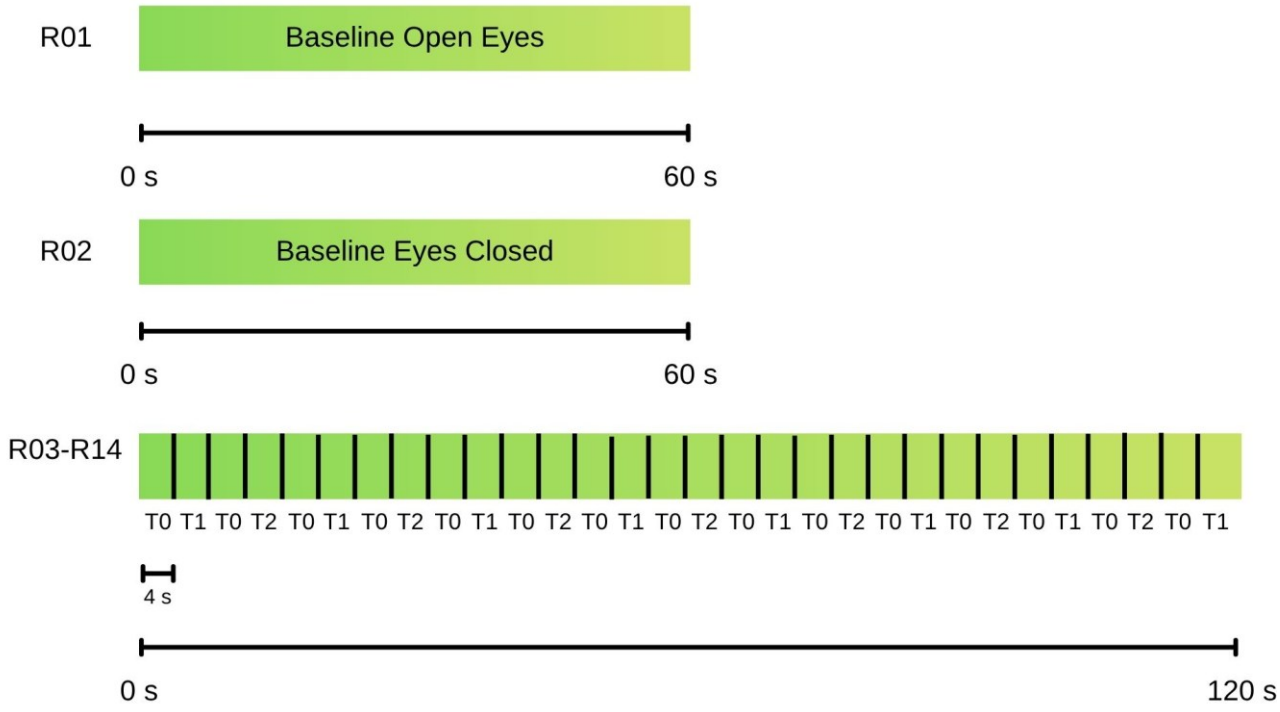

Figure 19. Timeline of the experimental protocol.

The EEG signals were recorded using a 64-channel montage based on the international 10-10 system (excluding electrodes Nz, F9, F10, FT9, FT10, A1, A2, TP9, TP10, P9, and P10) as shown in the Figure 20.

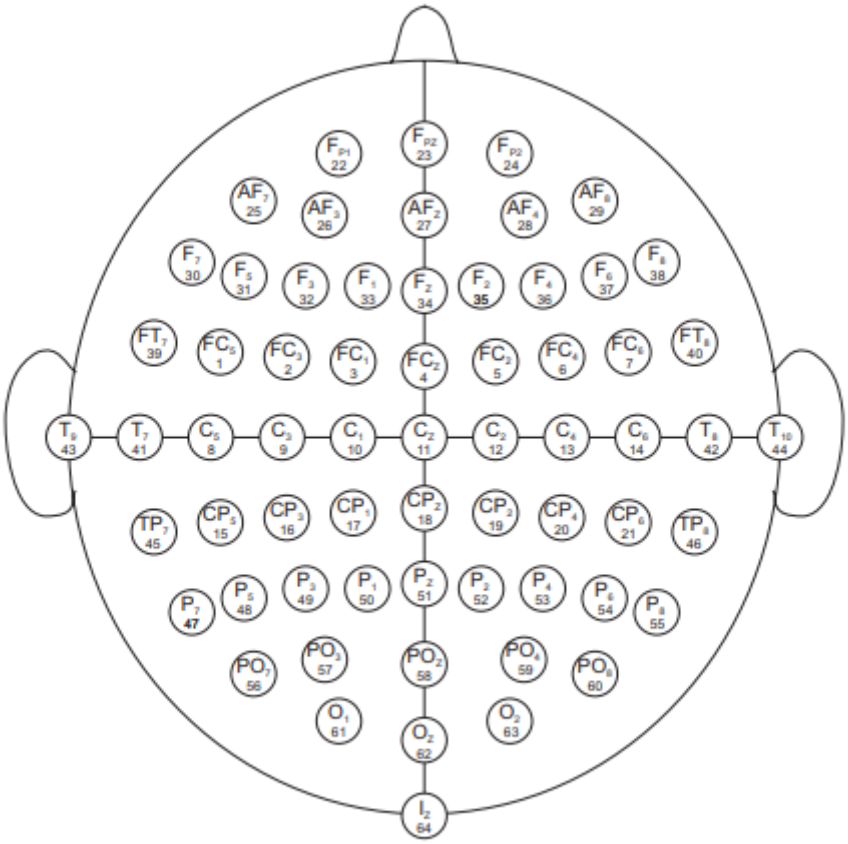

Figure 20. Electrode placement for the 64-channel montage used in the dataset.

The numbers below each electrode name indicate the order in which they appear in the records. Signals in the records are numbered from 0 to 63, while the numbers in the Figure 20. range from 1 to 64.

The data are provided in EDF+ (European Data Format Plus) format and contain: 64 EEG signals sampled at 160 Hz, providing adequate temporal resolution for capturing motor-related cortical dynamics and 1 annotation channel containing event markers. Event annotations are encoded as: T0 which corresponds to rest, T1 which corresponds to onset of motion (executed or imagery) of left fist (in runs 3, 4, 7, 8, 11, and 12) or both fists (in runs 5, 6, 9, 10, 13, and 14) and T2 which corresponds to onset of motion (execution or imagery) of the right fist (in runs 3, 4, 7, 8, 11, and 12) or both feet (in runs 5, 6, 9, 10, 13, and 14). These annotations are synchronized with the EEG signal and allow precise segmentation of trials for analysis. The dataset is organized in 109 subject folders, labeled from S001 to S109, each corresponding to each of the 109 participants. Within each folder there are EDF files representing the 14 experimental runs performed by the subject. Each file contains a complete EEG recording with 64 channels and synchronized event annotations. In addition to the

subject folders, the dataset includes several auxiliary files that support data interpretation and processing such as the ANNOTATORS which defines the event codes (T0, T1, T2), RECORDS which is a list of available recording files, SHA256SUMS.txt which is a Checksums for file integrity verification and wfdbcal which is a calibration file for compatibility with WFDB tools.

3.2 PRE-PROCESSING AND FEATURE EXTRACTION

In this work, the raw dataset was analyzed in MATLAB R2025a, using EEGLAB. EEGLAB is an interactive, menu-driven software environment for processing electrophysiological data, particularly EEG, running within the MATLAB programming environment. It provides an intuitive graphical user interface (GUI) that allows users to process data without requiring extensive programming experience. At the same time, for advanced users, all functions can be accessed via MATLAB scripts, and all data structures managed by the software are available in the MATLAB workspace, enabling full customization and automation of the analysis [44]. Among its key features, EEGLAB supports a wide range of import formats through the File-IO and BIOSIG interfaces, allowing the loading of various EEG file types. Furthermore, EEGLAB implements common signal processing methods, including filtering, re-referencing, independent component analysis (ICA), and time-frequency analysis. The ICLabel plugin is available for automatic classification of independent components into brain, muscle, eye, heart, line noise, and other artifact categories, facilitating the identification and removal of non-brain activity. The command history function further supports the transition from GUI-based exploration to the creation of batch scripts for reproducible and large-scale data analysis [45].

Once the data were imported into EEGLAB, the first step consisted of loading the electrode locations and defining the experimental conditions from the event markers. So, the channel locations were loaded using a standard 10-10 system cap file (Standard-10-10-Cap64.ced), which assigns 3D coordinates to each electrode for topographic mapping. For each subject and each run, the event triggers were extracted from the EEG files to identify distinct experimental conditions. For the baseline runs R01 and R02, we defined a single continuous task covering the entire run and labelled it as a rest condition while for the task runs R03 through R14, we used consecutive triggers to delimit individual trials. A specific class was then assigned to each trial based on the run number and trigger type: for runs R03, R07, and R11, trigger T1 corresponded to left hand execution and trigger T2 to right hand execution, while for runs R04, R08, and R12, the same triggers corresponded to left hand and right hand imagination respectively. For runs R05, R09, and R13, trigger T1 indicated both fists execution and trigger T2 both feet execution, while for runs R06, R10, and R14, the same triggers indicated imagination of the same movements.

The EEG data were then preprocessed to remove noise and artefacts; a bandpass filter was applied to the continuous EEG data with cutoff frequencies of 0.5 Hz (high-pass) and 70 Hz (low-pass), this frequency range was selected to remove slow drifts and DC offset (below 0.5 Hz) but also to remove high-frequency noise while preserving EEG activity of interest. Filtering was implemented using the *pop_eegfiltnew* function, which applies a linear finite impulse response (FIR) filter with Hamming window. Then, filtered data were re-referenced to the average of all channels using the *pop_reref* function. Powerline interference was addressed using the CleanLine plug-in to further remove powerline noise at 60 Hz, while to identify and remove non-neural artifacts, independent component analysis (ICA) was performed using the default *runica* algorithm from the EEGLAB toolbox; this algorithm decomposes the EEG signal into statistically independent components, each representing a distinct source of activity. Components were then classified using the ICLabel plug-in, a tool that automatically assigns each component the probability of belonging to seven possible classes, each representing a different signal source, such classes are “Brain”, “Muscle”, “Eye”, “Heart”, for what concerns biological sources, “Line Noise”, and “Channel Noise”, for what concerns non-biological sources, and “Other”. To automate the component rejection process in a systematic and objective manner, we applied predefined criteria: a component was labelled as artifact and removed if its probability of belonging to the “Brain” class was lower than 5%, or if its probability of belonging to any other class (excluding “Other”) was greater than 90%.

After the preprocessing steps, the continuous data were segmented into analysis windows and in particular, for the task runs R03 through R14, we used the trial boundaries defined by the triggers to segment the data into windows corresponding to the task periods (T1 and T2) and the rest periods (T0). While, the baseline runs R01 and R02, which lasted one minute each, were divided into non-overlapping windows of 4 seconds duration, matching the duration of the task intervals defined by consecutive triggers in the task runs. The baseline windows were assigned to class 1, the rest periods (T0) were assigned to class 2, while the task periods were assigned to the corresponding motor task classes (classes 3-10). Specifically, periods labelled as T1 or T2 were assigned to the following motor task classes: class 3 for left hand execution, class 4 for left hand imagery, class 5 for both fists execution, class 6 for both fists imagery, class 7 for right hand execution, class 8 for right hand imagery, class 9 for both feet execution, and class 10 for both feet imagery. This segmentation strategy ensured that only task-related activity was included in the motor execution and imagery analyses. For each window and for each channel, we computed the standard deviation of the signal: if four times the standard deviation exceeded 100 μV, the channel in that window was labelled as noisy. A window was considered as accepted if none of its channels exceeded this threshold; otherwise, it was marked as noisy and excluded from subsequent analyses. To systematically identify and remove unreliable

channels and runs, we applied predefined criteria: a channel was classified as non-reliable if more than 60% of the windows across the entire run were noisy; similarly, an entire run was marked as non-reliable if more than 60% of its channels were classified as non-reliable. This approach allowed us to obtain a detailed artefact profile for each channel and each window. For each accepted window, the power spectral density (PSD) was computed using Welch's method. This method divides each window into overlapping segments, multiplies each segment by a Hamming window, computes the periodogram of each segment using the Fast Fourier Transform, and then averages these periodograms. A 50% overlap between consecutive segments was used, and the number of FFT points was set to the next power of two greater than the segment length to optimize computation. From the power spectrum, 5 rhythms were extracted: Delta from 0.5 to 4 Hz, Theta from 4 to 8 Hz, Alpha from 8 to 12 Hz, sensorimotor rhythm (SMR) from 12 to 15 Hz, and Beta from 15 to 35 Hz. Next, to characterize each rhythm, the area under the PSD curve was calculated and the result for each window was reported into a matrix, where, any channel that had been flagged as noisy for that specific window had missing values for its features (NaN), ensuring that subsequent analyses would not be contaminated by noisy data. Then we calculated a set of 22 engagement indexes based on the equations provided in the literature [16].

Finally, a set of features like Event-Related Desynchronization (ERD), Frontal Alpha Asymmetry, Coherence and Phase Locking Value (PLV) have been calculated. The ERD was measured for the Alpha and Beta bands using the baseline run R01 as a reference. For each channel and each trial, the logarithmic ratio between task power and baseline power was calculated, yielding negative values for desynchronization and positive values for synchronization, so, ERD was nominally calculated for all 64 channels; however, if a channel was flagged as noisy in a given window, the corresponding ERD value was set to missing (NaN). Then, Frontal Alpha Asymmetry was computed as the difference between Alpha power at electrodes F4 and F3, divided by their sum: if either F3 or F4 was a noisy channel, the asymmetry value for that window was set to NaN. On the other hand, connectivity measures were computed for 27 symmetric electrode pairs defined according to the standard 10-10 montage. Midline electrodes (FPz, AFz, Fz, FCz, Cz, CPz, Pz, POz, Oz, Iz) were excluded from the analysis as they lack a distinct contralateral counterpart. While, for coherence estimation, Welch's averaged periodogram method was employed with Hamming windows and 50% overlap. For PLV, signals were bandpass-filtered using a zero-phase Butterworth filter to isolate the Alpha or Beta band, and the Hilbert transform was applied to extract the instantaneous phase. All connectivity measures were evaluated separately for the Alpha and Beta bands and exclusively on pairs of channels where both electrodes were artefact-free in the specific window.

3.3 FEATURE SET ORGANIZATION

Following the feature extraction step, all features were collected into a single two-dimensional feature matrix, where each row represented a single time window and each column represented a specific feature computed on a specific channel. The dataset was constructed by iterating over all subjects and all task runs (R03–R14), extracting exclusively the windows corresponding to T1 and T2 triggers, i.e., those in which the subject was actually performing or imagining the movement. Rest windows (T0) and baseline runs (R01–R02) were deliberately excluded, as they are not representative of the motor task of interest for classification. For each selected window, the following features were extracted and arranged in separate columns: spectral power for the five frequency bands (Delta, Theta, Alpha, SMR, Beta) for each of the 64 channels; the 22 engagement indexes, also per channel; ERD values for the Alpha and Beta bands, also per channel; frontal alpha asymmetry for the F4-F3 electrode pair; and connectivity measures (standard coherence, imaginary coherence, and PLV) for all 27 symmetric electrode pairs. To address missing values, a systematic data cleaning and imputation procedure was implemented. First, channels with an excessive proportion of missing values across all windows were identified and removed from the dataset, based on predefined thresholds. Subsequently, windows with a proportion of missing values exceeding a predefined threshold were discarded and the remaining missing values were then imputed using a subject-specific, region-based strategy. Then, for each subject, the scalp electrodes were grouped into six macro-regions based on both anatomical location and hemispheric lateralization: left and right frontal regions, left and right parietal regions, and left and right temporal regions. For each missing feature value in a given window, the median of the same feature type from all other channels within the same region and hemisphere, and from the same subject, was computed and used as the imputed value. If no valid values were available within the same region, the global median of that feature across all subjects was used as a fallback. After imputation, the dataset was organized into two distinct feature sets for classification: the first, referred to as the single-channel feature set, preserved the original feature values for each individual channel and each electrode pair, without any spatial aggregation, while the second, referred to as the region-aggregated feature set, was obtained by averaging, for each window and for each feature type, the values of all channels (and all electrode pairs for connectivity measures) belonging to the same macro-region. This procedure yielded a single aggregated value per region, per feature type, and per window, reducing the number of features. Both feature sets were then used independently in the classification stage.

3.4 CLASSIFICATION THROUGH MACHINE LEARNING

Following the dataset preparation procedure described in the previous section, a machine learning classification framework was implemented to evaluate the discriminability between ME and MI: for each subject and for each of the four analogous movement types (right hand, left hand, fists, and feet) a binary classification problem was defined between ME and MI. The four movement types were processed separately to preserve the specific neural activation patterns associated with each movement, as the somatotopic organization of the motor cortex implies distinct cortical representations for hand, fist, and feet movements. By maintaining separate binary problems for each movement type, we allowed the feature selection and classification algorithms to adapt to the specific discriminative features of each motor task, and this approach consistently yielded superior accuracy compared to a pooled strategy. The classification pipeline was applied separately to both the single-channel and the region-aggregated feature sets, to compare the impact of spatial aggregation on classification performance. In order to identify the most discriminative features while mitigating the risk of overfitting, a two-step feature selection procedure was applied for each movement type. First, a feature importance score was computed for each subject individually and then, an ensemble selection approach, referred to as the sum method, was adopted: features that were selected for at least 50% of the subjects, i.e., with a frequency greater than or equal to 0.5 times the number of subjects, were retained. This procedure yielded a subject-specific reduced feature set for each movement type. On this reduced feature set, two further selection steps were applied to optimize classification performance: removal of highly correlated features with a correlation threshold of 0.80 to address multicollinearity, and selection of the top 20 features based on the Wilcoxon rank-sum test to ensure statistical discriminability between ME and MI. Four classifiers were trained and evaluated: Linear Discriminant Analysis (LDA), Support Vector Machine (SVM) with linear kernel, SVM with radial basis function kernel, and Random Forest (RF). To evaluate the generalizability of the models, two cross-validation strategies were employed for each classifier and each movement type: 10-fold cross-validation and leave-one-subject-out (LOSO) cross-validation. In 10-fold cross-validation, (where the dataset was randomly partitioned into ten folds of approximately equal size), one fold was used as the validation set while the remaining nine folds served as the training set, and the process was repeated such that each fold served as the test set exactly once; the final performance metrics were obtained by averaging the results across all ten folds; while in LOSO cross-validation, the data from all subjects except one were used for training and the remaining subject was used for validation, repeated for each subject and this latter strategy is particularly important as it simulates the application of the classifier to new, unseen individuals. The performance was assessed using accuracy, sensitivity, specificity, and F1-score: accuracy represents the overall proportion of correct predictions across both

classes; sensitivity measures the proportion of correctly identified ME trials; specificity measures the proportion of correctly identified MI trials; and F1-score is the harmonic mean of precision and recall. The formal definitions of these metrics are reported in eq. (17), (18), (19) and (20):

$$Accuracy = \frac{TP + TN}{TP + TN + FP + FN} \tag{17}$$

$$Sensitivity = \frac{TP}{TP + FN} \tag{18}$$

$$Specificity = \frac{TN}{TN + FP} \tag{19}$$

$$F1 = 2 \cdot \frac{Precision \cdot Sensitivity}{Precision + Sensitivity} \tag{20}$$

where TP, TN, FP, and FN denote true positives, true negatives, false positives, and false negatives, respectively, with ME trials defined as the positive class and MI trials as the negative class. For each correlation threshold, the best-performing classifier was identified based on these metrics.

4. RESULTS

The feature extraction and cleaning procedure yielded an initial dataset of 18,834 windows and 1,874 features, with an overall proportion of missing values of 27.98%. To address those missing values, a systematic data cleaning and imputation procedure was implemented: first, the sources of missing values were investigated at the channel level and fifteen channels were identified as not clean and were removed from the dataset. Specifically, channels FC4, FC6, FC2, C5, FT8, and C3 exhibited features with more than 60% missing values across all windows, while T9, T7, C1, O1, O2, PO8, PO7, CP4, and P8 showed features with more than 35% of NaN across all the windows as well. This channel-level removal reduced the feature space from 1,874 to 1,397 features and decreased the overall NaN proportion to 21.59%. After removing those 15 channels and discarding windows with more than 10% missing values, the dataset was reduced to 11,292 windows and 1,397 features, with no residual missing values and the number of subjects retained was 98 out of the original 109.

A general overview of the classification performance across all four movement types reveals that the Random Forest classifier consistently emerged as the top performer under 10-fold cross-validation for both feature sets, while LDA and linear SVM delivered intermediate results. In contrast, the radial basis function SVM systematically failed, exhibiting near-zero sensitivity and extremely low F1-scores across most configurations. Moreover, a performance decrease was observed when moving from 10-fold to LOSO cross-validation across all classifiers and movement types, indicating that the models learned subject-specific patterns that did not generalize to unseen individuals. Region-aggregated features consistently outperformed single-channel features under 10-fold cross-validation, with accuracy improvements; however, this advantage largely disappeared under LOSO validation, suggesting that spatial aggregation may enhance within-subject discriminability at the expense of cross-subject generalizability. Finally, performance was relatively comparable across the four movement types, with no single movement showing a marked advantage over the others, although feet movements tended to achieve the highest accuracies. The classification results right hand movement are reported in Table 6 for 10-fold cross-validation and in Tables 7 for LOSO cross-validation.

Table 6. Right hand: 10-fold cross-validation results.

Single-channel	Classifier	Acc (%)	Sens (%)	Spec (%)	F1 (%)
	LDA	58.17	51.97	64.11	54.85
	SVM Linear	57.96	38.98	76.12	47.55
	SVM RBF	54.93	31.82	77.03	40.84
	Random Forest	59.89	51.75	67.67	55.78
Region-aggregated	**LDA**	56.32	49.64	62.71	52.63
	SVM Linear	56.75	48.54	64.59	52.32
	SVM RBF	51.39	2.19	98.46	4.22
	Random Forest	62.53	56.20	68.58	59.46

Acc: accuracy; Sens: sensitivity; Spec: specificity; F1: F1-score.

Table 7. Right hand: LOSO cross-validation results.

Single-channel	Classifier	Acc (%)	Sens (%)	Spec (%)	F1 (%)
	LDA	57.21	50.80	63.34	53.72
	SVM Linear	57.00	37.37	75.77	45.94
	SVM RBF	53.14	29.34	75.91	37.98
	Random Forest	56.32	49.42	62.92	52.52
Region-aggregated	**LDA**	53.71	48.10	59.08	50.40
	SVM Linear	54.10	46.57	61.31	49.80
	SVM RBF	51.11	1.61	98.46	3.11
	Random Forest	52.14	46.35	57.68	48.64

Acc: accuracy; Sens: sensitivity; Spec: specificity; F1: F1-score.

For the left hand movement, the sum method selected 283 features from 2,904 windows. The same general trends observed for the right hand movement were confirmed for the left hand movement, Random Forest again achieved the highest 10-fold cross-validation accuracies while LOSO cross-validation produced systematically lower performances across all classifiers. The classification results for the left hand movement are reported in Table 8 for 10-fold cross-validation and in Table 9 for LOSO cross-validation.

Table 8. Left hand: 10-fold cross-validation results.

Single-channel	Classifier	Acc (%)	Sens (%)	Spec (%)	F1 (%)
	LDA	60.09	53.22	66.62	56.51
	SVM Linear	60.50	43.53	76.63	51.79
	SVM RBF	60.19	37.95	81.33	48.16
	Random Forest	61.36	52.79	69.51	57.11
Region-aggregated	**LDA**	56.99	52.86	60.91	54.50
	SVM Linear	57.58	53.07	61.85	54.94
	SVM RBF	51.45	0.71	99.66	1.40
	Random Forest	65.01	58.66	71.05	62.03

Acc: accuracy; Sens: sensitivity; Spec: specificity; F1: F1-score.

Table 9. Left hand: LOSO cross-validation results.

Single-channel	Classifier	Acc (%)	Sens (%)	Spec (%)	F1 (%)
	LDA	59.71	52.72	66.35	56.05
	SVM Linear	59.64	42.69	75.76	50.76
	SVM RBF	57.99	36.25	78.64	45.68
	Random Forest	58.16	50.39	65.55	53.99
Region-aggregated	**LDA**	54.86	50.81	58.70	52.31
	SVM Linear	55.03	50.60	59.23	52.30
	SVM RBF	51.21	0.14	99.73	0.28
	Random Forest	53.62	45.58	61.25	48.92

Acc: accuracy; Sens: sensitivity; Spec: specificity; F1: F1-score.

For the fists movement, the sum method selected 283 features from 2,751 windows. The classification results followed the same overall patterns established for the upper limb movements: Random Forest outperformed the other classifiers under 10-fold cross-validation, while the RBF SVM again produced lower accuracy with minimal sensitivity. The classification results for the fists movement are reported in Table 10 for 10-fold cross-validation and in Table 11 for LOSO cross-validation.

Table 10. Fist: 10-fold cross-validation results.

Single-channel	Classifier	Acc (%)	Sens (%)	Spec (%)	F1 (%)
	LDA	59.40	42.03	74.36	48.93
	SVM Linear	57.47	25.53	84.98	35.71
	SVM RBF	58.56	29.69	83.42	39.87
	Random Forest	61.72	47.92	73.61	53.67
Region-aggregated	**LDA**	58.27	43.28	71.18	48.98
	SVM Linear	58.09	36.68	76.52	44.75
	SVM RBF	53.94	0.47	100.00	0.94
	Random Forest	63.47	49.65	75.37	55.71

Acc: accuracy; Sens: sensitivity; Spec: specificity; F1: F1-score.

Table 11. Fist: LOSO cross-validation results.

Single-channel	Classifier	Acc (%)	Sens (%)	Spec (%)	F1 (%)
	LDA	57.22	38.26	73.55	45.28
	SVM Linear	56.56	24.19	84.44	34.01
	SVM RBF	55.73	26.32	81.06	35.49
	Random Forest	57.22	41.24	70.97	47.15
Region-aggregated	**LDA**	55.73	39.83	69.42	45.43
	SVM Linear	55.73	33.07	75.24	40.87
	SVM RBF	53.73	0.00	100.00	0.00
	Random Forest	52.31	35.19	67.05	40.58

Acc: accuracy; Sens: sensitivity; Spec: specificity; F1: F1-score.

For the feet movement, the sum method selected 283 features from 2,835 windows and the classification results that were largely consistent with the general patterns observed for the hand and fist movements. The classification results are reported in Table 12 for 10-fold cross-validation and in Table 13 for LOSO cross-validation.

Table 12. Feet: 10-fold cross-validation results.

Single-channel	Classifier	Acc (%)	Sens (%)	Spec (%)	F1 (%)
	LDA	58.48	42.42	72.72	48.98
	SVM Linear	57.18	26.58	84.30	36.84
	SVM RBF	56.72	23.80	85.89	34.07
	Random Forest	59.93	48.72	69.86	53.33
Region-aggregated	**LDA**	56.72	41.74	69.99	47.54
	SVM Linear	56.47	36.56	74.12	44.11
	SVM RBF	53.02	0.08	99.93	0.15
	Random Forest	67.13	56.31	76.71	61.68

Acc: accuracy; Sens: sensitivity; Spec: specificity; F1: F1-score.

Table 13. Feet: LOSO cross-validation results.

Single-channel	Classifier	Acc (%)	Sens (%)	Spec (%)	F1 (%)
	LDA	57.81	41.37	72.39	47.95
	SVM Linear	56.30	25.38	83.70	35.30
	SVM RBF	54.96	19.67	86.23	29.09
	Random Forest	55.17	43.17	65.80	47.50
Region-aggregated	**LDA**	53.54	37.99	67.33	43.45
	SVM Linear	54.14	33.41	72.52	40.64
	SVM RBF	52.98	0.00	99.93	0.00
	Random Forest	52.56	39.11	64.47	43.65

Acc: accuracy; Sens: sensitivity; Spec: specificity; F1: F1-score.

5. DISCUSSION

The preprocessing pipeline was designed to obtain clean and reliable EEG signals while preserving the neurophysiological information relevant to motor tasks. A bandpass filter between 0.5 Hz and 70 Hz was applied to remove slow drifts and DC offsets below 0.5 Hz, which are not of neural origin, as well as high-frequency noise while preserving the EEG frequency bands of interest. Also, ICA was employed to identify and remove non-neural artifacts; the ICA decomposition, combined with the ICLabel plugin, enabled for the automatic classification of independent components into seven categories: brain, muscle, eye, heart, line noise, channel noise, and other. Component rejection was intentionally conservative: components with a brain probability lower than 5% or a non-brain probability higher than 90% were discarded, while components with uncertain classification were retained to minimize the risk of removing physiologically relevant neural activity. This approach is particularly important in MI paradigms, where frontal and central components may contain both neural and ocular activity, making aggressive artifact rejection potentially detrimental to the preservation of meaningful EEG signals.

Regarding the decision to exclude the gamma band from the analysis, this was dictated by the sampling rate of the EEG data (160 Hz): reliable estimation of gamma activity typically requires a sampling rate of at least 250–500 Hz to achieve a sufficient number of samples per cycle, and the gamma band is often defined up to 70–100 Hz in the literature. With a 160 Hz sampling rate, the Nyquist frequency would be 80 Hz, which is insufficient to represent gamma frequencies above 70 Hz without aliasing. Moreover, the limited number of samples per cycle would compromise the accuracy of power spectral density estimates in the gamma range. This limitation motivated the focus on lower frequency bands (delta, theta, alpha, SMR, and beta) and on engagement indexes that do not involve gamma power in their formulation. Moreover, for the computation of the ERD, the selection of the R01 run (eyes open) as the baseline was motivated by the need for a reference condition that matches the visual and attentional state of the task runs, all of which were performed with eyes open; using an eyes-open baseline minimizes physiological differences not directly related to the experimental conditions, thereby making the feature estimation more fair to the motor processes under investigation. Also, a key methodological choice in this study was the adoption of a hemispherically separated region-aggregation strategy inspired by approaches documented in the literature: the electrodes were grouped into six regions to preserve the lateralized nature of motor-related EEG activity. This choice was motivated by the need to maintain the contralateral activation patterns that are fundamental to discriminating between unilateral hand movements. The

hemispheric separation is particularly critical for the right and left hand movements, which exhibit clear contralateral dominance in the sensorimotor cortex.

The imputation procedure was implemented primarily to retain a sufficient amount of data for analysis, preventing the aggressive removal of data, while still ensuring the reliability of the resulting feature matrix. After discarding noisy channels and excluding windows with more than 10% missing features, the proportion of NaN values in the remaining dataset was extremely low. This justified the use of imputation as a reasonable and controlled strategy, allowing the preservation of a substantially larger dataset without compromising its overall quality. In addition to the imputed dataset, a second version of the dataset was created for comparative purposes and discussed here for completeness. This dataset, referred to as the zero-NaN dataset, was obtained by retaining only those windows that contained no missing values starting from the original dataset of 18,834 windows and 1,874 features, i.e., windows with 0% NaNs across all features. The same 15 problematic channels previously identified were removed first, then, all windows with at least one NaN value were discarded: this conservative approach resulted in a dataset of 4,659 windows, 1,397 features, and 72 subjects, with an overall NaN proportion of 0%. This zero-NaN dataset was used as a benchmark to evaluate the impact of imputation on classification performance. The comparison between the zero-NaN and imputed datasets provides important insights into the impact of imputation on classification performance and the trade-off between data quantity and quality: the higher performance observed on the zero-NaN dataset confirms that imputation, despite its careful design, introduces, even if extremely low, a degree of variability that can alter discriminative information. However, it is important to note that the zero-NaN dataset is substantially smaller in terms of both windows and subjects, which may limit the generalizability of the findings. Interestingly, the narrowing of the performance gap under LOSO cross-validation suggests that the imputation procedure did not substantially alter the subject-specific variability that limits generalization performance, and that the additional subjects and windows included in the imputed dataset did not translate into improved generalization. This finding aligns with observations in the literature, where inter-subject variability is consistently identified as a primary factor limiting BCI performance across various paradigms [23,24]. In fact, in 10-fold cross-validation, the zero-NaN dataset outperformed the imputed one, suggesting that imputation introduces a slight distortion. However, under LOSO cross-validation, this performance gap disappeared, this means that when the model faces a new, unseen subject, the differences between individuals become the primary challenge, rendering the minor distortion from imputation negligible. More specifically, for the zero-NaN dataset, the Random Forest classifier achieved 10-fold cross-validation accuracies ranging from 66.96% to 68.29% across the four movement types, with the feet movement yielding the best performance (69.25%). Under LOSO

cross-validation, the performance dropped to 54.98–60.53%, highlighting the impact of inter-subject variability.

One of the most striking findings of this study is the significant drop in performance from 10-fold cross-validation to LOSO cross-validation across all classifiers and movement types. This consistent drop indicates that the models are substantially affected by subject-specific variability in the EEG signals; in other words, the patterns that discriminate between ME and MI are not fully consistent across subjects, and models trained on one set of subjects do not generalize well to a new, unseen subject. This is a well-known challenge in EEG-BCI research, often referred to as the cross-subject generalization problem. The fact that the drop is observed even with region-aggregated features, which were intended to reduce the impact of local artifacts and capture more robust patterns, suggests that the subject-specific variability is not simply due to noisy single-channel measurements, but reflects fundamental differences in the neural patterns associated with ME and MI across individuals. This is supported by the literature [26], which has shown that individual differences in cortical anatomy, functional organization, and behavioral strategies contribute to the variability in EEG signals during motor tasks. If models trained on one set of subjects do not generalize well to new subjects, then a significant amount of calibration data is required for each new user, which limits the usability of the system. This suggests that a calibration phase, in which the system is adapted to the specific neural patterns of each individual, remains necessary for achieving reliable BCI control. The drop in LOSO performance is particularly concerning for BCI applications that aim to be "plug-and-play" without extensive user-specific training. The magnitude of the drop observed in this study is consistent with previous studies on EEG-based motor decoding that have reported drops of 10–20 percentage points when moving from within-subject to cross-subject validation [28,29].

The decision to process each movement type separately in the classification was not only neurophysiologically motivated but also empirically validated: preliminary analyses revealed that pooling data from all four movement types into a single framework produces lower classification performances, likely due to the high variability in spatial activation patterns across different motor effectors. This finding is consistent with the somatotopic organization of the motor cortex, where different body parts are represented in distinct cortical areas, and suggests that classification algorithms perform better when they are allowed to learn movement-specific discriminative patterns rather than attempting to capture a common representation across all movements [19]. The classification performance varied across the four movement types, with the feet movement generally yielding the highest performance, particularly with region-aggregated features on the imputed dataset and this result is consistent with the somatotopic organization of the sensorimotor cortex: the cortical

representation of the feet is located medially, near the midline, while hand and fist representations are more lateral. As a consequence, EEG electrodes positioned over the midline (e.g., Cz) are more directly aligned with the neural sources generating foot-related activity, potentially resulting in more focal and consistent EEG patterns compared to the more lateral representations of the hands. This interpretation is supported by the literature on EEG-based motor decoding, where foot movements have been shown to elicit more distinct and reproducible patterns than hand movements [30]. In contrast, the fists movement may involve more complex coordination of multiple muscle groups, resulting in more variable neural patterns that are harder to classify, additionally, this movement requires bilateral coordination, which may introduce additional sources of variability that complicate the discrimination between ME and MI. The right and left hand movements produce more variable patterns due to the involvement of the contralateral hemisphere [32].

To contextualize the classification performance obtained in this study, it is useful to compare our results with those reported in the literature. However, a direct comparison must account for the fundamental difference in the classification problem addressed: Pérez-Velasco et al. [17] reported a classification accuracy of 86.21% for left/right hand discrimination using a deep learning approach (EEGSym) on the same PhysioNet dataset. It is important to clarify that this accuracy refers to a binary classification task (left vs. right hand) performed under a transfer learning scenario: the model was trained on ME data and tested on MI data. Therefore, this result does not address the classification between ME and MI for the same movement type but rather the lateralization of the movement (left vs. right) across different task conditions. Fazli et al. [42] reported an EEG-alone accuracy of 78.2% for left/right hand discrimination during motor imagery, with a 5% average improvement when combining EEG with NIRS, observed in over 90% of subjects. Both studies addressed a task that exploits the strong spatial separation of cortical activation across the two hemispheres, distinguishing between left and right hand movements, which is less complex than the ME vs MI discrimination on all the four different type of movements. In contrast, our task required distinguishing whether a movement was executed or imagined for the same limb, lacking such a robust spatial discriminant. This fundamental difference in task complexity explains the discrepancy in accuracy between the studies and highlights the greater challenge associated with classifying the nature of motor activity rather than its lateralization. It is worth noting that the classification of ME vs MI for the same movement type is a more challenging problem because both conditions involve similar neural substrates, with differences manifesting primarily in the amplitude and timing of ERD/ERS patterns rather than in the spatial localization of the activation [38]. This observation might initially appear to contrast with our earlier finding that pooling data from all four movement types produced lower classification performance than processing each movement type separately. However, there is no

actual contradiction: the two observations refer to different sources of variability. Within the same movement type (e.g., right hand ME vs right hand MI), the neural patterns are spatially similar, making it difficult to discriminate between execution and imagery based on spatial features alone; the classifier must rely on subtle differences in signal amplitude and timing. Across different movement types (e.g., right hand vs feet), the neural patterns are spatially distinct due to the somatotopic organization of the motor cortex, where different body parts are represented in different cortical areas [19]. When movements are pooled together, the classifier must account for both the subtle differences between ME and MI within each movement type and the large spatial differences between movement types. This increased variability makes the classification problem more complex and results in lower performance, as confirmed by our preliminary analyses. Therefore, while the challenge of distinguishing ME from MI lies in the temporal and amplitude differences within the same movement, the challenge of pooling multiple movements lies in the spatial differences across movements. Processing each movement type separately allows the classifier to focus on the subtle ME vs MI differences without being confounded by the large spatial variability across different motor effectors. Therefore, the accuracies achieved in this study, while modest compared to left/right discrimination tasks, represent a meaningful contribution to the literature on EEG-based discrimination of motor execution and motor imagery, addressing a fundamentally more difficult problem. Nevertheless, the inherent difficulty of this task, combined with the cross-subject variability suggests that EEG-only approaches may benefit from multimodal integration. The inclusion of complementary signals, such as hemodynamic responses measured by fNIRS or muscular activity measured by EMG, could provide additional discriminant dimensions that are not available from EEG alone [43]. Moreover, fNIRS could offer more stable subject-independent features due to the greater consistency of cerebral hemodynamics across individuals.

6. CONCLUSION

The aim of this study was to investigate whether a comprehensive set of EEG-derived features could effectively discriminate between motor execution (ME) and motor imagery (MI) using machine learning techniques. The feature set comprised the spectral power of five EEG rhythms (Delta, Theta, Alpha, SMR, and Beta), 22 engagement indexes, event-related desynchronization (ERD) in the Alpha and Beta bands, frontal alpha asymmetry, and three connectivity measures: standard coherence, imaginary coherence, and phase-locking value and PLV. The analysis was conducted on a publicly available dataset from the PhysioNet repository comprising 109 healthy performing four different types of motor task, right hand, left hand, both fists, and both feet, both imagined and executed. The results obtained confirm the intrinsic complexity of the classification task between ME and MI, in fact, the best performance, achieved with the Random Forest classifier under 10-fold cross-validation using region-aggregated features, reached an accuracy of 67.13% for feet movements, with an F1-score of 61.68%. Although these values are above chance level, they remain moderate, indicating that the electrophysiological separability between the two conditions is subtle and not trivial. A particularly significant finding was the marked drop in performance observed when moving from 10-fold cross-validation to leave-one-subject-out (LOSO) cross-validation, with accuracies decreasing to approximately 52–54% across all movement types; this highlights the critical challenge of cross-subject generalization, suggesting that the neural patterns discriminating between ME and MI are highly subject-specific. This finding aligns with the existing literature and underscores that inter-subject variability remains one of the primary obstacles to the development of reliable brain–computer interfaces (BCIs). It also suggests that a calibration phase, tailored to each individual user, may still be necessary to achieve satisfactory decoding performance in practical applications.

The study underlines that EEG-based discrimination between motor execution and motor imagery is a challenging task, influenced by multiple factors including feature selection, classification algorithm, movement type, and, most importantly, inter-subject variability. The results highlight the need for advanced signal processing strategies, robust feature extraction, and the development of domain generalization methods that can effectively transfer knowledge across individuals. The Random Forest classifier emerged as the most effective among the tested algorithms, confirming its suitability for handling high-dimensional EEG data and selecting informative features. Future work should focus on the adoption of deep learning architectures specifically designed for EEG signals, combined with transfer learning and domain adaptation techniques, that may offer a promising pathway toward overcoming the cross-subject generalization barrier. Ultimately, the findings of this thesis contribute to a deeper understanding of the electrophysiological differences between motor execution and motor

imagery, providing a foundation for the development of more reliable and user-independent BCI systems for motor rehabilitation and assistive technologies.

BIBLIOGRAPHY

[1] Ambrosi G, Cantino D, Castano P, Correr S, D'Este L et al. Anatomia dell'uomo. Edi. Ermes. 2006. 2.

[2] Vanputte C, Regan J, Russo A, Seeley R, Stephens T et al. Anatomia Umana. Sorbona. 2018. 4.

[3] Mainardi L, Ravazzani P. Principi di bioelettricità e biomagnetismo. Pàtron Editore. 2011.

[4] Van Putten M. Dynamics of Neural Networks: A Mathematical and Clinical Approach. Springer-Verlag Berlin and Heidelberg GmbH & Co. KG. 2020.

[5] Beniczky S, Schomer D. Electroencephalography: basic biophysical and technological aspects important for clinical applications. Epileptic Disorders (2020);22:697-715.

[6] Casson A, Yates D, Smith S, Duncan J, Rodriguez-Villegas E. Wearable Electroencephalography. IEEE Engineering in Medicine and Biology Magazine (2010);29:44-56.

[7] Di Flumeri G, Aricò P, Borghini G, Sciaraffa N, Di Florio A et al. The Dry Revolution: Evaluation of Three Different EEG Dry Electrode Types in Terms of Signal Spectral Features, Mental States Classification and Usability. Sensors (2019);19:1365.

[8] Grigg-Damberg M, Foldvary-Schafer Nancy. Sleep-Related Epilepsy and Electroencephalography. Sleep Medicine Clinics (2012);7:xiii-xiv.

[9] Bos D. EEG-based Emotion Recognition. The Influence of Visual and Auditory Stimuli (2006);56:1-17.

[10] Seeck M, Koessler L, Bast T, Leijten F, Michel C et al. The standardized EEG electrode array of the IFCN. Clinical Neurophysiology (2017);128:2070-2077.

[11] Hyvärinen A. Independent component analysis: recent advances. Philosophical Transactions of the Royal Society A Mathematical, Physical and Engineering Sciences (2012);371.

[12] Nalwaya A, Das K, Pachori R. Emotion identification from TQWT-based EEG rhythms. AI-Enabled Smart Healthcare Using Biomedical Signals. 2022.

[13] Kropotov J. The enigma of infra-slow fluctuations in the human EEG. Frontiers in Human Neuroscience (2022);16.

[14] Cheyne D. MEG studies of sensorimotor rhythms: A review. Experimental Neurology (2013);245:27-39.

[15] Krishnakumaran R, Ray S. Temporal characteristics of gamma rhythm constrain properties of noise in an inhibition-stabilized network model. Cerebral Cortex (2023);33:10108-10121.

[16] Marcantoni I, Assogna R, Del Borrello G, Di Stefano M, Morano M, et al. Ratio Indexes Based on Spectral Electroencephalographic Brainwaves for Assessment of Mental Involvement: A Systematic Review. Sensors (2023); 23.

[17] Pérez-Velasco, S., Marcos-Martínez, D., Santamaría-Vázquez, E., Martínez-Cagigal, V., & Hornero, R. (2024). Bridging motor execution and motor imagery BCI paradigms: An inter-task transfer learning approach. Computers in Methods and Programs in Biomedicine, 246, 108048.

[18] Al-Quraishi, M. S., Ali, S. S. A., Saleh, H. H., & AbouOmar, M. S. (2023). Variations in EEG signals across different brain regions during motor imagery and execution tasks. Computers in Methods and Programs in Biomedicine, 228, 107209.

[19] Chepurova, A., & Kurkin, S. (2021). Comparison on brain activity for mechanical imagery and execution: a brief review. IEEE DCNA, 2021. https://doi.org/10.1109/DCNA53427.2021.9587202

[20] Xu L, Zhang H, Hui M, Long Z, Jin Z, Liu Y, Yao L. Motor execution and motor imagery: A comparison of functional connectivity patterns based on graph theory. *Neuroscience* (2014);261:184–195.

[21] Duann, J.-R., & Chiou, J.-C. (2016). A comparison of independent event-related desynchronization responses in motor-related brain areas to movement execution, movement imagery, and movement observation. PLoS ONE, 11(9), e0161965. doi:10.1371/journal.pone.0161965

[22] Nakayashiki, K., Saeki, M., Takata, Y., Hayashi, Y., & Kondo, T. (2014). Modulation of event-related desynchronization during kinematic and kinetic hand movements. Journal of NeuroEngineering and Rehabilitation, 11, 90. doi:10.1186/1743-0003-11-90

[23] Pfurtscheller G, Lopes da Silva FH. Event-related EEG/MEG synchronization and desynchronization: basic principles. Clinical Neurophysiology, 1999.

[24] Carrillo-de-la-Peña, M. T., Lastra-Barreira, C., & Galdo-Álvarez, S. (2006). Limb (hand vs. foot) and response conflict have similar effects on event-related potentials (ERPs) recorded during motor imagery and overt execution. European Journal of Neuroscience, 24(1), 1–12. https://doi.org/10.1111/j.1460-9568.2006.04926.x

[25] Srinivasan R, et al. EEG coherence. In Encyclopedia of Neuroscience, 2009.

[26] Nolte G, et al. Identifying true brain interaction from EEG data using the imaginary part of coherency. Clinical Neurophysiology, 2004.

[27] Lachaux JP, et al. Estimating the time-course of coherence between single-trial brain signals. NeuroImage, 1999.

[28] Varela F, et al. The brainweb: phase synchronization and large-scale integration. Nature Reviews Neuroscience, 2001.

[29] Davidson RJ. Anterior cerebral asymmetry and the nature of emotion. Brain and Cognition, 1992.

[30] Coan JA, Allen JJB. Frontal EEG asymmetry as a moderator and mediator of emotion. Biological Psychology, 2004.

[31] Carrillo-de-la-Peña, M. T., Galdo-Álvarez, S., & Lastra-Barreira, C. (2008). Equivalent is not equal: Primary motor cortex (MI) activation during motor imagery and execution of sequential movements. Brain Research, 1226, 134–143. https://doi.org/10.1016/j.brainres.2008.05.089

[32] World Stroke Organization. Global Stroke Fact Sheet 2022. Geneva: WSO; 2022.
[33] Lawrence ES, et al. Estimates of the prevalence of acute stroke impairments and disability in a population-based cohort. Stroke (2001);32(6):1280–1285.
[34] World Health Organization. Spinal Cord Injury – Key Facts. WHO Fact Sheets (latest available update). Geneva: WHO.
[35] Hardiman O, et al. Amyotrophic lateral sclerosis. Nature Reviews Disease Primers (2017);3:17071.

[36] Bauer, R., Fels, M., Vukelić, M., Ziemann, U., & Gharabaghi, A. (2015). Bridging the gap between motor imagery and motor execution with a brain–robot interface. NeuroImage, 108, 149–157. https://doi.org/10.1016/j.neuroimage.2014.12.026

[37] Zhi, H., Yu, T., Gu, Z., Lin, Z., Che, L., Li, Y., & Yu, Z. (2022). Supervised contrastive learning-based domain generalization network for cross-subject motor decoding. IEEE Transactions on Neural Systems and Rehabilitation Engineering, 30, 2080–2091. https://doi.org/10.1109/TNSRE.2022.3192930

[38] Xu, K., Huang, Y.-Y., & Duann, J.-R. (2025). The sensitivity of single-trial mu-suppression detection for motor imagery performance as compared to motor execution and motor observation performance. Frontiers in Human Neuroscience. https://doi.org/10.3389/fnhum.2025.01432

[39] Guttmann-Flury, E., Sheng, X., & Zhu, X. (2023). Channel selection from source localization: A review of four EEG-based brain–computer interfaces paradigms. Behavior Research Methods, 55(5), 1980–2003. https://doi.org/10.3758/s13428-022-01897-2

[40] Amemiya, K., Ishizu, T., Ayabe, T., & Kojima, S. (2010). Effects of motor imagery on intermanual transfer: A near-infrared spectroscopy and behavioural study. Brain Research, 1343, 149–158. https://doi.org/10.1016/j.brainres.2010.04.048

[41] Fu, Y., Chen, R., Gong, A., Qian, Q., Ding, N., Zhang, W., Su, L., & Zhao, L. (2021). Recognition of flexion and extension imagery involving the right and left arms based on deep belief network and functional near-infrared spectroscopy. Computational Intelligence and Neuroscience, 2021, 1–12. doi:10.1155/2021/5598289

[42] Fazli, S., Mehnert, J., Steinbrink, J., Curio, G., Villringer, A., Müller, K.-R., & Blankertz, B. (2012). Enhanced performance by a hybrid NIRS–EEG brain computer interface. NeuroImage, 59(1), 519–529. doi:10.1016/j.neuroimage.2011.07.084

[43] G. Schalk, D. J. McFarland, T. Hinterberger, N. Birbaumer, and J. R. Wolpaw, "EEG Motor Movement/Imagery Dataset," PhysioNet, 2009. doi: 10.13026/C28G6P. https://doi.org/10.13026/C28G6P

[44] Delorme A, Makeig S. EEGLAB: an open source toolbox for analysis of single-trial EEG dynamics including independent component analysis. *Journal of Neuroscience Methods*, 2004;134(1):9-21.

[45] Pion-Tonachini L, Kreutz-Delgado K, Makeig S. ICLabel: An automated electroencephalographic independent component classifier, dataset, and website. *NeuroImage*, 2019;198:181-197.